Summertime sediment storage on the Alaskan Beaufort Shelf and implications for ice-sediment rafting and shelf erosion

Eidam, E.F.[1]

[1]College of Earth, Ocean, and Atmospheric Sciences, Oregon State University, Corvallis, OR

AUTHOR'S NOTE: This paper is a non-peer-reviewed preprint version which has been submitted to EarthArXiv for early access. It was submitted to JGR-Oceans for peer review in March 2025.

Key Points:

- Winds regulate sediment transport by generating upwelling and downwelling on the shelf (and concurrent wave resuspension)
- Prevailing easterly winds promote sediment convergence/storage on the inner shelf during the open-water season
- Sediment trapped on the inner shelf is available for sea-ice entrainment in the fall and then rafting in the spring, promoting shelf erosion

Corresponding author: Emily Eidam, `emily.eidam@oregonstate.edu`

Abstract

Arctic coastlines are known to be rapidly eroding, but the fate of this material in the coastal ocean (and the sedimentary dynamics of Arctic continental shelves in general) is less well-constrained. This study used summertime mooring data from the Alaskan Beaufort Shelf to study sediment-transport patterns which are dominated by waves and wind-driven currents. Easterly wind events account for most of the seasonal sediment transport, and serve to focus sediment on the inner shelf. This is a key finding because it means sediment is readily available for wave-driven resuspension and sea-ice entrainment during fall storms. Sediment-ice entrainment has been previously implicated as a major mechanism for Arctic Shelf erosion–and so the summertime focusing of sediment observed in this study may actually serve to enhance shelf erosion rather than promote shelf sediment accumulation. In a pan-Arctic context, the Alaskan Beaufort shelf is somewhat similar to the Laptev Sea Shelf, where previous work has shown that sediment is also focused during the summer months (but for different reasons related to estuarine-like circulation under the Laptev plume). The Alaskan Beaufort example contrasts with previous work on the Canadian Beaufort Shelf, where dominant winds from the opposite direction (northwest) likely promote strong seaward dispersal of sediment rather than inner-shelf convergence. This study thus highlights the importance of understanding dominant wind patterns when considering seasonal and inter-annual storage, transport, and erosion of sediments from Arctic continental shelves.

Plain Language Summary

Arctic coastal erosion is well-studied, but where does the sediment go in the ocean? This study investigates how waves and currents transport sediments on the Alaskan Beaufort shelf. The goal is to better understand whether sediment is removed from the continental shelf or stored on the shelf during the summer when sea ice retreats. Strong winds, which occur every few days, create downwelling (seaward) currents during westerly winds and upwelling (landward) currents during easterly winds. Because easterly winds are dominant, sediments are generally transported landward during the summer. Intuitively this should lead to long-term storage of sediment on the shelf, but other work has shown that the shelf (inshore of 15-20 m depth at least) is eroding. A likely explanation (building on previous researchers' findings) is that sediment stored during the summer on the inner shelf is mixed into the water column and incorporated into new sea ice during autumn

storms – and then rafted into deeper water in ghe spring. In short, summertime transport of sediment toward shore puts the sediment in a good position to be eroded, entrained in sea ice, and removed from the shelf the following year – thus representing a likely mechanism for Arctic continental shelf erosion.

1 Introduction and Background

From the perspective of marine sedimentology, Arctic continental shelves are unique among global systems. In the Alaskan and Siberian sectors, shelf breaks occur at ∼40-100 m water depth in many locales, which make these systems shallow relative to a typical global shelf break depth of ∼130 m (a depth which corresponds to the sea-level lowstand during the Last Glacial Maximum; e.g., Harris & Macmillan-Lawler, 2016). Shelf widths vary around the Arctic from the relatively narrow Alaskan Beaufort Shelf at <100 km to the Laptev sector of the Siberian shelf, which is the widest in the world at ∼1200 km (Herman, 1974). Due largely to the wide Siberian shelf, continental shelves comprise 30-50% of the total area of the Arctic Ocean (Macdonald et al., 1998; Jakobsson et al., 2003). These shallow, low-relief ocean margins lie at an interesting intersection between wintertime ice forces, which may be of waning importance in the next decades to centuries due to Arctic reductions in sea ice (Perovich & Richter-Menge, 2009), and wave forces, which are gaining strength as a consequence of the reduced sea ice (e.g., Thomson et al., 2016). Sediment routing, storage, and erosion are presently influenced by both ice and wave forces, and so changes in these forces will have interesting ramifications for seabed properties and water-column (and related) dynamics.

Globally, rivers are the dominant source (∼95%) of modern sediment to continental shelves (Syvitski et al., 2003). In most shelf environments, these sediments are reworked by fairweather waves, currents, storms, and sometimes sediment-gravity flows to form deposits on the shelf or off-shelf deep-sea archives (e.g., P. S. Hill et al., 2007). By contrast, fluvial sediment yields (the amount delivered per basin area) in the Arctic are quite low due to cold-weather conditions on adjacent landscapes and previous scouring of sediments by ice sheets (Milliman & Meade, 1983; Syvitski, 2002). However, rates of coastal erosion along soft-sediment coastlines (primarily in Siberia, Alaska, and parts of Canada) are some of the highest in the world, with mean rates of 0.5 m/yr and localized rates as high as 20 meters per year (Lantuit et al., 2012; Gibbs & Richmond, 2017). These fast rates are driven by degradation of ice-rich permafrost soils. Consequently, bluff erosion provides a substantial source of sediment which exceeds fluvial supply as much as tenfold in some regions (Rachold et al., 2000; Reimnitz et al., 1988). It is worth noting here that glaciers provide additional sediment supply to regional coastlines, notably in Greenlandic fjords and some regions of the Canadian Archipelago–but much of that sediment is trapped in fjords (which are not the subject of this paper).

Because temperatures in the Arctic are warming rapidly (Rantanen et al., 2022), it is logical to assume that sediment loads from eroding coasts and rivers will increase throughout the Siberian to Alaskan sector of the Arctic as well as soft-sediment coasts in the Canadian Archipelago. In the last few decades, erosion rates have already accelerated in some regions (e.g., Jones et al., 2009; Piliouras et al., 2023) with potential implications for nutrient release (Nielsen et al., 2022). Arctic river discharge is also increasing in many systems (e.g., Feng et al., 2021), and while there is debate about whether sediment loads have also increased (see Syvitski, 2002; Doxaran et al., 2015; Holmes et al., 2002), it is reasonable to assume this may happen since sediment load tends to scale with river discharge (Milliman & Meade, 1983) and sediment yields tend to scale with temperature (Syvitski & Morehead, 1999).

But where does sediment derived from coasts and rivers go? This question has been relatively well-answered for systems at diverse other latitudes, but different processes are at work in the Arctic. Sea ice protects Arctic shelves from waves for 7-9 months per year, but sea ice also causes local wintertime gouging of the seafloor. Offshore pack ice and nearshore landfast collide over the continental shelf and create large pressure ridges; the subaqueous "keels" below these ridges scour the seafloor to depths of a meter or more (Kovacs & Mellor, 1974; Barnes et al., 1984; Rearic, 1982). In the spring, rivers often deliver a majority of their sediment load to the coast while sea ice is still present, and river waters can flow over and/or under the ice (Arnborg et al., 1967; Reimnitz & Bruder, 1972; Okkonen & Laney, 2021). Modeling work has shown that the remnant sea ice causes fluvial sediments to be routed and deposited farther offshore than if ice were absent (Cooper et al., 2024). During the summer, wind-driven currents together with waves (which are limited in size due to fetch limitations from pack ice in the basin) provide sediment-transport energy akin to a normal lower-latitude shelf environment. But in the fall (and occasionally in the winter), strong storms generate sediment resuspension at the same time that ice is forming, leading to sea-ice entrainment of sediment (e.g., Kempema & Reimnitz, 1989). These sediments are often rafted away to distal locations, causing a uniquely polar type of sediment advection. Recent work on bathymetric change detection and Pb-210 isotope profiles has demonstrated that the inner shelf is eroding at rates up to 3 m in 70 years in Harrison Bay (and slower rates elsewhere; Heath, 2024; Zimmermann et al., 2022). Reimnitz et al. (1988) hypothesized that entrainment of sediment in sea ice may be sufficient

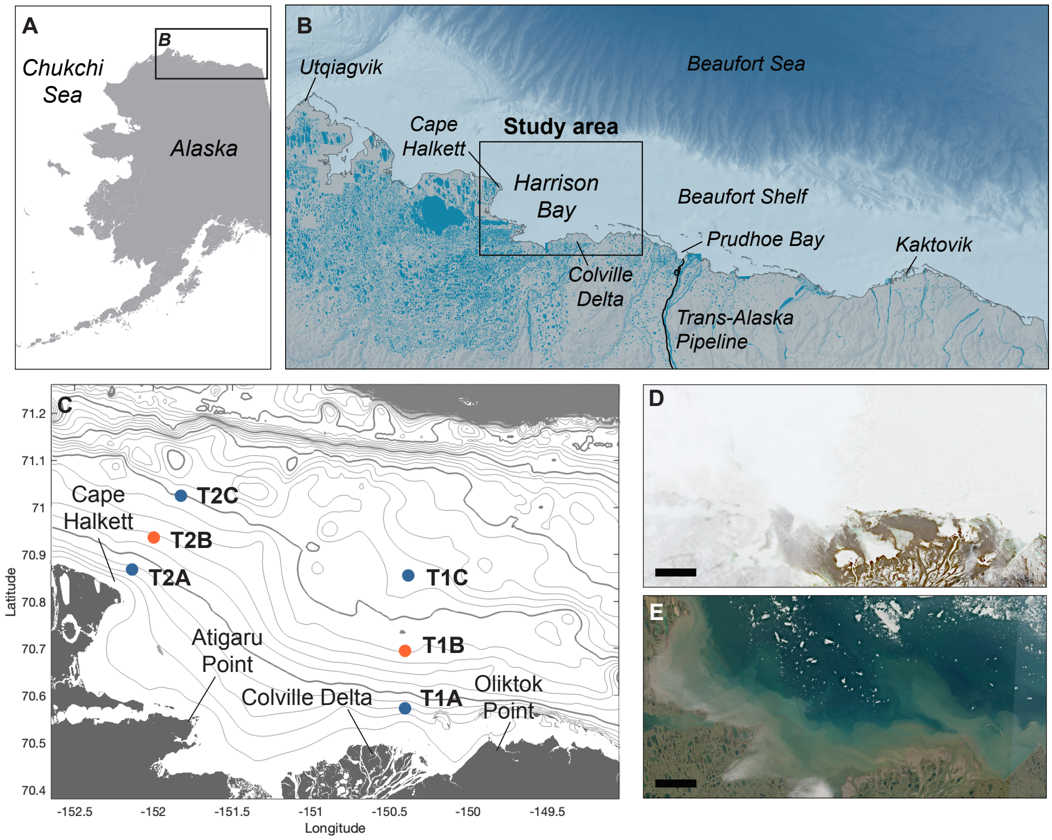

Figure 1: Vicinity map and example plume images. A) Regional map. B) North Slope map. C) Study area map showing locations of summer 2022 mooring deployments. Bathymetric contours were derived from the International Bathymetric Chart of the Arctic Ocean (IBCAO); light lines are 2 m and dark lines are 10 m. D) Colville River plume image from May 2023. E) Colville River plume image from July 2023. Scale bars in each satellite image represent 10 km. (*Satellite images are from Copernicus/Sentinel-2*).

to remove the annual input of sediments from bluffs and rivers, but estimates of sediment budgets in sea ice have been historically difficult to make.

This study presents summertime vessel-based and mooring observations collected in 2021 and 2022 from Harrison Bay, Alaska in order to better describe sediment-transport characteristics and sediment trajectories during the open-water season on the Alaskan Beaufort Shelf. The results are further contextualized based on a trend analysis of wind and wave dynamics from a 70-year ERA5 hindcast record. This expanded analysis highlights the dominance of easterly and northeasterly winds, with implications for sediment focusing on the inner shelf.

2 Regional setting

The Alaskan Beaufort Shelf is a relatively narrow, low-gradient passive margin which borders the North Slope of Alaska, a broad coastal plain on the northern edge of the Brooks Range. In Harrison Bay, the shelf is approximately 70-90 km wide and has a compound (stepped) shelf break at ∼40-m and 70-m water depths (Fig. 1). The coastal plain, which comprises relict marine terraces from past high stands in sea level as well as old fluvial deposits, is characterized by permafrost soils and thermokarst topography (e.g., Farquharson et al., 2016). The presence of these ice-rich soils promotes rapid coastal erosion rates of ∼2.5-18.6 m/yr (Reimnitz et al., 1988; Gibbs & Richmond, 2017). Bluff erosion can be mechanical (driven by wave energy) and/or thermal (driven by relatively warm seawater which thaws ground ice). Erosion is a somewhat cyclical process each year. Bluffs begin to thaw in the early summer, and material is released and removed by waves throughout the summer and fall – with the strongest removal generally occurring during large fall storms (Gibbs et al., 2019).

The Colville River delivers an estimated $\sim 5.9 \times 10^{10}$ kg of sediment per year to the shelf, and more than half of this load may be delivered within a period of weeks during spring breakup (Arnborg et al., 1967). Muddy plume waters emanating from the Colville are visible in satellite imagery from early spring (Fig. 1D), but by mid summer the fluvial sediment concentrations have decreased and coastal resuspension plumes in the western part of the bay exhibit stronger concentrations (Fig. 1E).

The Beaufort Shelf is covered by sea ice for ∼8-9 months per year (October/ November to June), and sediment transport in this and similar regions is likely minimal during this time (Weingartner et al., 2017; P. R. Hill et al., 1991). The outer edge of the shelf is near the southern limb of the Beaufort Gyre, a cyclonic current (Rudels & Carmack, 2022). A shelfbreak jet flows counter to the gyre in an eastward direction (except during some storm events), but is generally located along the continental slope at depths greater than the shelf (Aagaard, 1984; Pickart, 2004; Pickart, Spall, & Mathis, 2013). During the open-water season (approximately late June through early October), winds can generate relatively strong currents. When storms in the North Pacific and Bering Sea drive easterly winds (at Pt. Barrow) greater than 4 m/s, upwelling is established on the slope (Schulze & Pickart, 2012). Storms from the Bering Sea, Siberia, or Arctic basin episodically bring westerly winds which drive downwelling (Foukal et al., 2019). The region is microtidal with tidal ranges <20 cm (Okkonen, 2016; this study).

Winds are dominantly from the northeast or east (Fig. 2). This trend is illustrated in five years of Prudhoe Bay weather station data (Fig. 2A; NBDC, 2025) and corresponding ERA5 climate reanalysis data (Fig. 2B; Hersbach et al., 2023; Section 3.2), but the Prudhoe Bay observation data also illustrate some strong westerly storms which are absent from the ERA5 products. The wave climate builds throughout the open-water season (June to October) as a result of seasonal sea-ice retreat and the associated seasonal increase in fetch (Fig. 2C,D; e.g., Hošeková et al., 2021). Typical significant wave heights on the shelf (illustrated by mooring data) and farther offshore (illustrated by ERA5 data) are on the order of 0.5-2 m with occasional peaks of up to ~4 m (Fig. 2C). Peak wave periods are ~2-10 s (Fig. 2D).

Seabed sediments are quite diverse in terms of texture and small-scale morphologies. Sediments at many nearshore sites are well-sorted sands, but mud is often present in the form of a mud drape, mud clasts and lenses within the sand, or mud balls (Reimnitz et al., 1977; Eidam et al., 2025). Sands also occur in sporadic locations across the shelf. The diversity is attributed largely to ice scouring effects which plow the seafloor. Based on clay mineralogy analyses, sediments are generally supplied by nearby sources with some mixing from the various regional rivers (Naidu & Mowatt, 1983).

Researchers investigated shallow inner-shelf sediment transport dynamics in Harrison Bay to some degree during the 1970s and 1980s when oil extraction infrastructure was being developed. For example, strong bedload transport rates in water depths of <10 m were inferred after an artificial gravel island lost 25% of its mass during the first winter after construction (Barnes & Reiss, 1983). Researchers also noted that 4-m-deep strudel scours (pits formed by jet-like flows of springtime river overflow through ice cracks) near the Colville Delta were infilled within 2-3 years. They estimated westerly bedload transport rates (dictated by dominant wind directions) of 40,500 m^3/yr in a 4.5-km wide swath of the Harrison Bay nearshore zone (Reimnitz & Kempema, 1982).

The fate of finer-grained sediments in Arctic shelf settings is more complex. In the Canadian Beaufort Sea (near the Alaskan border), northwesterly winds create sea-level setup and strong pressure gradients which drive downwelling flows of water and seaward transport of sediment on the inner shelf, especially where the shelf is backed by a bluff

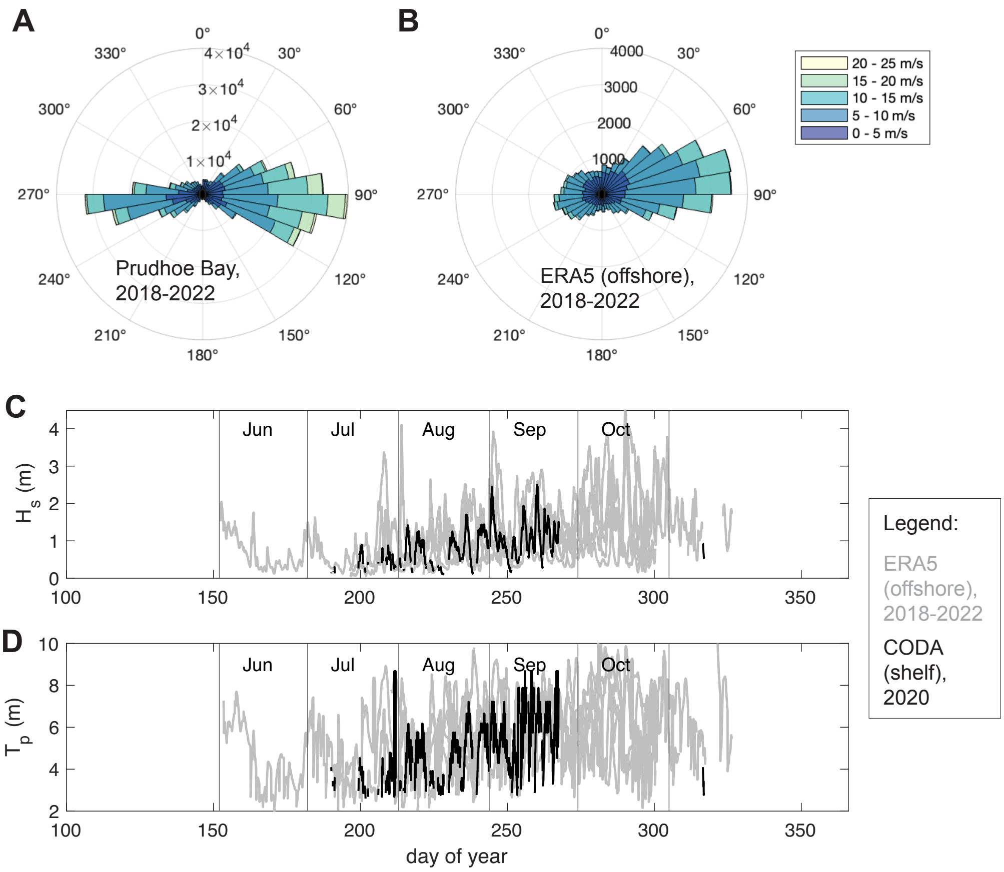

Figure 2: Typical regional wind and wave conditions (between 2018 and 2022). A) Wind rose from Prudhoe Bay weather station data. B) Wind rose from ERA5 hindcast data at an offshore site. C) Significant wave heights from ERA5 data for 2018-2022 (gray) for an offshore site and from CODA (Coastal Ocean Dynamics in the Arctic study) mooring data (Hošeková et al., 2021) in 2022 (black). See text for details. D) Same as (C) but for peak wave period.

that can enhance the setup (as opposed to a barrier island which allows washover; Héquette & Hill, 1993; Hequette & Aernouts, 2010). On the Laptev Shelf in Siberia, the Laptev plume transports sediment seaward during the summer, but sediment settles into a landward-flowing bottom layer in what has been described as a "quasi-estuarine sediment circulation" (meaning a two-layer flow with landward return flow near-bed; Wegner et al., 2005). This leads to focusing of sediment on the middle shelf during summer. Wind events can cause cause sediment transport in both on-shelf and off-shelf directions, however; strong northerly winds can drive southward transport, while strong southwesterly winds can drive northeastward transport (at ∼30-40 m depth; Wegner et al., 2013). The results presented in this paper address summertime sediment-transport dynamics on the Alaskan Beaufort shelf, which complement studies from Siberia and Canada to provide a panorama of similar wind-dominated sediment transport across a range of pan-Arctic settings (including shelves of different widths subject to different dominant wind directions).

3 Methods

The primary data presented in this study are mooring data which were collected from six sites in Harrison Bay during August 2022. Moorings were deployed and recovered from the 14-m coastal vessel *R/V Ukpik*. Vessel-based ADCP data, water-column profile measurements, and water samples were collected in 2022 as well as an earlier survey in summer 2021; these data are described elsewhere (Eidam, Cooper, et al., 2023) and are referenced here for context about summertime water masses present in the bay. The same moorings deployed in 2022 were also deployed on the Colville Delta front for ∼9 days in 2021 (due to unfavorable ice conditions) but those data are not presented here (see Eidam et al., 2022).

Other measurements were also collected in 2021 and 2022, including multibeam bathymetry, seabed grab samples, short sediment cores, and portable free-fall penetrometer measurements. These data are addressed in other publications (Heath et al., 2024; Eidam, Thomson, et al., 2023; Brilli, 2022; Eidam et al., 2025). Time-series data from agency archives are included for context where useful, including river discharge data (described in Appendix A), wind data (described in Appendix B), and ERA5 hindcast data of winds and waves (described in Section 3.2 and Appendix C).

3.1 Mooring data

Small moorings were deployed along two cross-shelf transects for a month-long period between early August and early September 2022 (Fig. 1). A brief summary of mooring locations and deployment dates is provided in Table 1, while detailed information about deployment schemes is provided in Table D1 (Appendix D). Mooring locations were chosen to capture "inner," "middle," and "middle/outer" shelf dynamics (at sites denoted A, B, and C, respectively), while avoiding deployments in locations that were more than 40 km from shore (presuming that sediment-transport signals would be weak beyond that). These locations corresponded to depths of approximately 8-9, 17, and 20-24 meters, respectively. The T1 line was located due north of the Colville Delta where some river influence was anticipated, and the T2 line was located near Cape Halkett (∼55-70 km west of the T1 line; Fig. 1). The goals of the mooring deployments were to assess cross-shelf and and along-shelf gradients and variability in suspended-sediment concentrations, transport vectors, and forcing mechanisms (wave- and current-driven advection and resuspension). Additional information about mooring configurations is provided in Appendix D).

Table 1: Deployment locations, times, and parameters measured for small moorings (2022). The parameters are as follows: S = salinity; T = temperature; P = pressure (depth); Tu = turbidity; TSS = total suspended solids (derived from turbidity); Vel = velocity (profile).

Station	Lat (°N)	Lon (°W)	Depth (m)	Deploy date, time (UTC)	Recover date, time (UTC)	Days deployed	Parameters measured
T1A	70.572	-150.400	8.8	8/1/2022 17:00	9/2/2022 21:15	32	S, T, P, Tu (& TSS)
T1B	70.695	-150.401	17.4	8/1/2022 18:30	9/2/2022 22:00	32	Vel, P, TSS
T1C	70.856	-150.381	24.3	8/1/2022 19:45	9/2/2022 23:15	32	P, Tu (& TSS)
T2A	70.869	-150.134	8.4	8/3/2022 19:00	9/3/2022 21:15	31	S, T, P, Tu (& TSS)
T2B	70.936	-151.999	17.0	8/3/2022 20:15	9/3/2022 19:30	31	Vel, P, TSS
T2C	71.025	-151.827	19	8/3/2022 21:45	9/3/2022 21:00	31	P, Tu (& TSS)

Bed stresses were calculated using Nortek-brand Aquadopp (ADCP) sensor data from the T1B and T2B sites. The Madsen wave-current interaction model was used (see Madsen, 1994), which applies the Law of the Wall when waves are absent and a non-linear combined stress formula when waves are present. The wave-current interaction model requires the wave orbital velocity (u_{bm}), wave angular frequency (ω), current speed (u_z) at a known height above bed (z), angle between waves and currents (ϕ), and bed roughness length (z_0). For this study we calculated u_{bm} as a function of the significant wave height and peak wave period obtained from the Aquadopp, per the following equation (e.g., Soulsby, 1987; Wiberg & Sherwood, 2008):

$$u_{bm} = \frac{\pi H}{T \sinh(kh)} \tag{1}$$

where H is the wave height (m), T is the wave period (s), k is the dimensionless wave number, and h is water depth (m). The wave angular frequency is simply $2\times\pi/T$. For ϕ, the exact value of the wave-current angle was not readily known, but values of both 0° and 90° were tested and found to yield only ∼3-6% difference in the τ results. A value of $\phi = 0°$ was thus used which produced slightly higher values than for $\phi = 90°$ and thus more conservative estimates of the stress needed to mobilize sediments. The current speed at height z = 0.9 m above the bed was used for u_z (this height corresponded the first good bin of velocity data).

In hydrodynamically rough flows, z_0 is calculated from $d_{50}/12$, where d_{50} is the median grain diameter measured using a bed sediment sample from the study site. Sediments sampled from across the bay exhibited a wide diversity of sediment sizes and textures including intercalated mud and sand, mud balls, and compacted sediments (Eidam et al., 2025). Sediments in the vicinity of T1B tended to be sandy, and sediments at T2B tended to be muddy. For T1B, 0.4 was assumed for z_0; this value was suggested by Soulsby (1997) for unrippled sands, and lies between lower values of 0.2 for mud and 0.3 for sand/shell mixtures and a higher value of 0.7 for mixed mud/sand. For T2B, 0.2 was used to represent mud. These values could arguably be fine-tuned, but because no detailed sediment transport-rate calculations have been made from the data, these approximations seem adequate.

Optical backscatter sensors were installed on each mooring at elevations of $\sim$20 cm or 54 cm within the bottom boundary layer (see Table D1). Sensors were calibrated in the laboratory using sediments collected from the study area (see Appendix E). Measurements from sensors mounted at 54 cm above bed (cmab) were converted to measurements at a reference elevation of 20 cmab using a Rouse profile, in order to allow for comparison of TSS values between sensors (see Appendix F).

3.2 Historical wind and wave reanalysis data from ERA5

In order to lend a longer-timescale context to the observational data presented in this study, ERA5 reanalysis data dating back to the 1940s-1950s were downloaded from the Copernicus data repository (Hersbach et al., 2023). Data were obtained from location 151°N, 71.5°E which represents a site seaward of the study area on the continental slope at 1485 m water depth—in other words, a location where deep-water wave mechanics are in effect. Data included easterly and westerly wind speed at 10 m above the surface, peak wave periods, significant wave heights (of combined wind waves and swell), significant heights of wind waves, and significant heights of swell. Wind stresses were calculated from these data according to Equations B1 and B2 provided in Appendix B. Wave-driven bed stresses were calculated from the wave period and height data as described in Appendix G.

4 Results

4.1 River, wind, and hydrodynamic conditions during the mooring period

During the mooring period (30 Jul to 5 Sep 2022), the Colville River discharge ranged from ∼160 to 1720 m^2/s at Umiat (Fig. 3A). Based on the rating curved derived from 1960s in situ measurements (Appendix A), these discharges corresponded to sediment concentrations of approximately 3-100 mg/L. The estimated suspended-sediment flux from the river was 1.30×10^8 kg ($\sim1.4\times10^5$ tons).

Winds were dominantly easterly or westerly with variables speeds of ∼5-10 m/s (Fig. 3B). Between Aug 6 and 14, winds were primarily from the west/northwest with moderate speeds of <10 m/s (Fig. 3B). An easterly wind event (with speeds of up to 15 m/s) occurred around August 21-24 and generated the strongest wind stresses during the mooring period (directed westward). Water levels, which oscillated based on semidiurnal tides (with a tidal range of ∼20 cm), decreased to ∼30-40 cm below the mean water level for the period of record during this event (Figs. 3D, 4A). A coastal setdown of up to ∼10 cm was generated between mooring stations A and C on Transect 1 (Fig. 3C), and ∼7 cm between stations A and C on Transect 2 (Fig. 4A). In the along-shelf dimension, water levels were roughly 7 cm lower at T1B than at T2B (Fig. H1). Following this event, winds reversed direction while river discharge remained somewhat high, and a somewhat smaller coastal setup was generated on both transects.

Near-bed salinities ranged from 24 to 30 PSU at T1A (Fig. 3E) and 26 to 30 PSU at T2A (Fig. 3B). Temperature was inversely related to salinity; warmer temperatures accompanied fresher water. Temperatures at T1A ranged from -1 to 4°C (Fig. 3E) and temperatures at T2A ranged from -1 to 6°C (Fig. 3B).

Water-column velocity profiles at T1B exhibited shearing ∼5-6 m and 10-11 m below the surface (Fig. 3F,G). Surface currents were generally directed eastward during coastal setup events (and westerly winds) and westward during coastal setdown events (and easterly winds). The maximum measured currents occurred during the late August wind event and were ∼0.7 m/s near the surface at T1B. Near-bed currents were <0.3 m/s throughout the mooring deployment, and were directed northeastward (slightly offshore) during setup events southwestward (onshore) during setdown events (Fig. 3F,G).

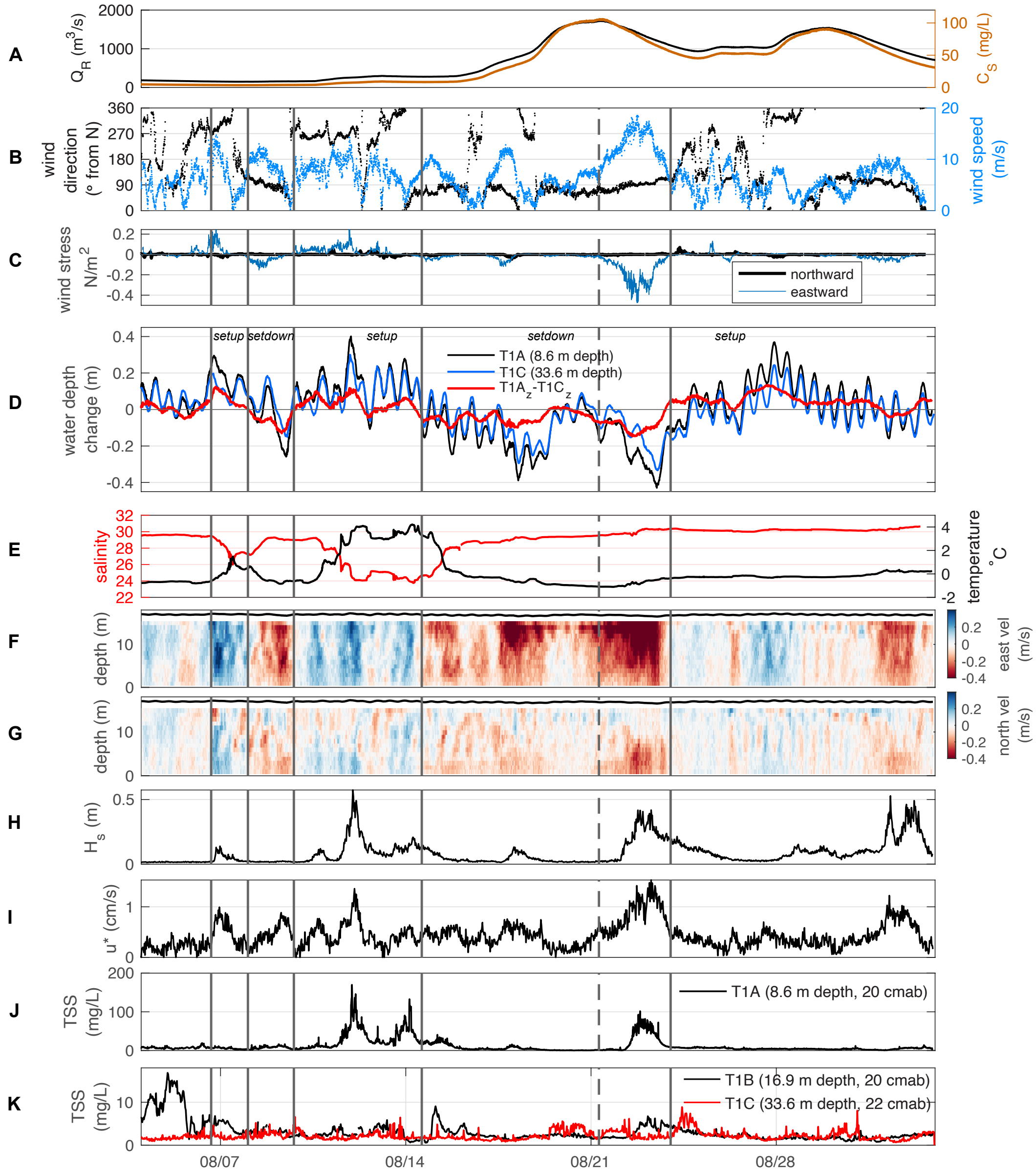

Figure 3: River, wind, and T1 mooring data (2022). A) Colville River discharge and sediment flux (based on USGS gauge and rating curve; see text). B,C) Wind direction, speed, and stress from NWS station PRDA2 at Prudhoe Bay (see text). D) Water-level changes at T1A and T1C. E) Near-bed salinity and temperature at T1A. F,G) Up-looking east and north velocity profiles at T1B. H) Significant wave height at T1B. I) Combined wave-current shear velocity at T1B. J,K) Near-bed TSS at T1A, T1B, and T1C.

Water-column velocity profiles at T2B were truncated in the upper water-column due to limited range of the sensor, but currents in the lower half of the water column followed similar patterns as currents at T1B. Early in the record at T2B, setup events caused northeastward bottom current flow, and setdown events caused southwestward flow. The strong wind event in late August caused strong southwestward flow near-bed.

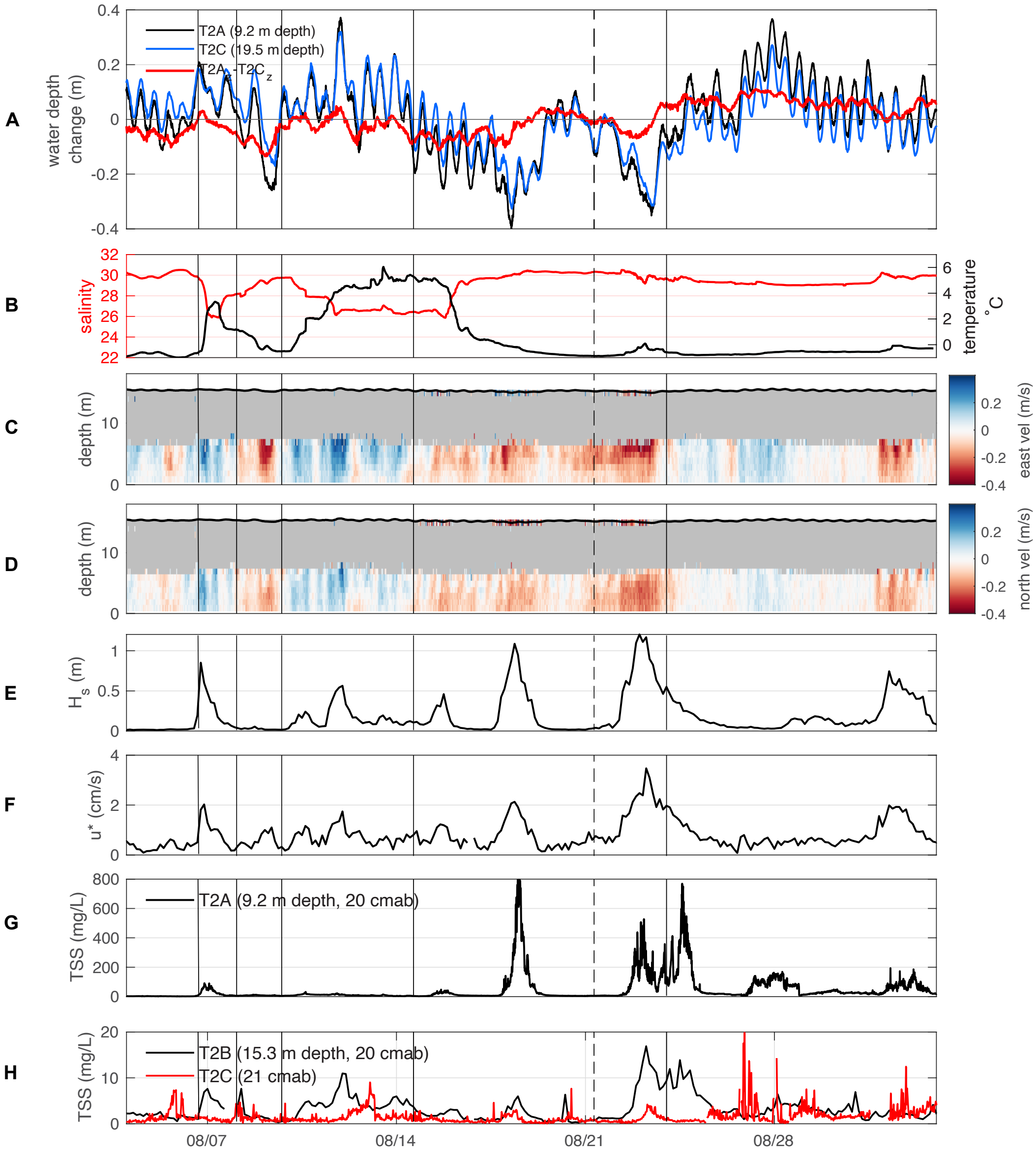

Figure 4: Mooring results from T2 (2022). A) Water-level changes at T2A and T2C. B) Near-bed salinity and temperature at T2A. C,D) Up-looking east and north velocity profiles at T2B (note that upper water-column data are truncated due to a range limit on the sensor). E) Significant wave height at T2B. F) Combined wave-current shear velocity at T2B. G,H) Near-bed TSS at T2A, T2B, and T2C.

Significant wave heights at T1B and T2B were typically less than 0.2 m except during wind events. Westerly winds of ∼12 m/s on 11-12 August generated 0.5-m high waves at both sites. Strong easterly winds on 18 Aug and 23 Aug generated waves >1 m high at T2B, but interestingly only generated ∼0.5-m waves at T1B on 23 Aug.

Combined wave-current shear velocities exceeded 1 cm/s (a nominal threshold of motion for sand; Miller et al., 1977) when wave heights exceeded ∼0.5 m at both sites.

During the rest of the record, u^* was generally less than 0.8 cm/s (Figs. 3I, 4F). At T1B, bed stress was generally dominated by currents but waves helped create the strongest stresses (Fig. J1). At T2B, where wave energy was stronger, waves dominated the bed stress signal at most times.

4.2 Suspended-sediment dynamics and transport during the mooring period

Strong gradients in TSS were observed in both the across-shelf and along-shelf directions. On the T1 transect, TSS values sampled at 20 cmab at T1A exceeded 100 mg/L during strong wave events, while values at T1B were less than 10 mg/L (representing more than an order of magnitude reduction between the 9-m and 17-m isobaths; Fig. 3J, K). On the T2 transect, peak TSS values were >500 mg/L at T2A and ∼15 mg/L at T2B, which represented more than an order of magnitude decrease between the 9 and 15 m isobaths (Fig. 4G,H). TSS values at T2C (at 19 m water depth) were less than 10 mg/L and typically several times smaller those measured at T2A. It is worth noting that the strongest bed stresses at T2B did not necessarily produce the strongest TSS signals (Fig. 4F,G).

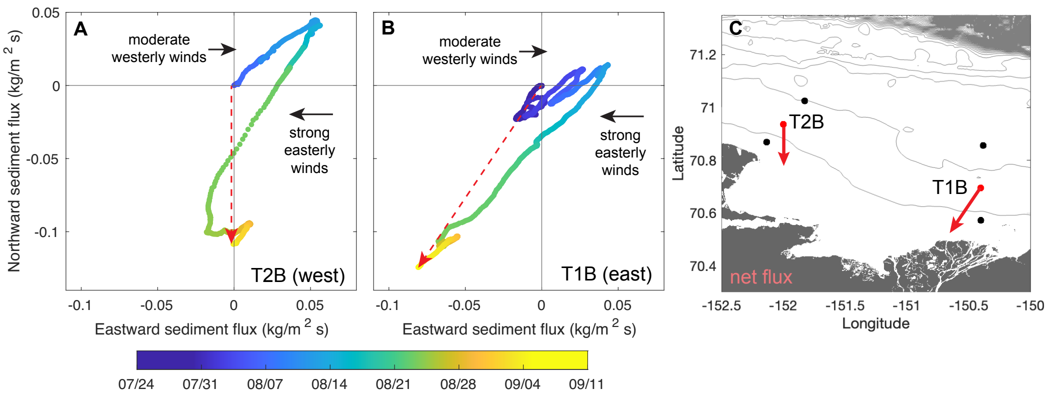

Figure 5: Sediment flux vectors. A) Cumulative sediment flux at site T2B during the mooring deployment. The axes represent the sediment mass concentration (kg/m^3) multiplied by the nearbed velocity (m/s) (see text for more details). The red dashed arrow denotes the representative net transport of a hypothetical particle that started at the origin. B) Same as (A) for site T1B. C) Map of net sediment flux vectors from (A) and (B) plotted on the respective mooring sites with appropriate east/north scaling.

Sediment fluxes at each middle-shelf site (T1B and T2B) varied on timescales similar to the reversals in wind directions (Fig. 5). During westerly winds, sediment transport vectors (which were approximated as the TSS at 0.54 cmab times the velocity at at 0.9 mab) were directed northeastward, or obliquely off-shelf (Fig. 5A). During easterly winds,

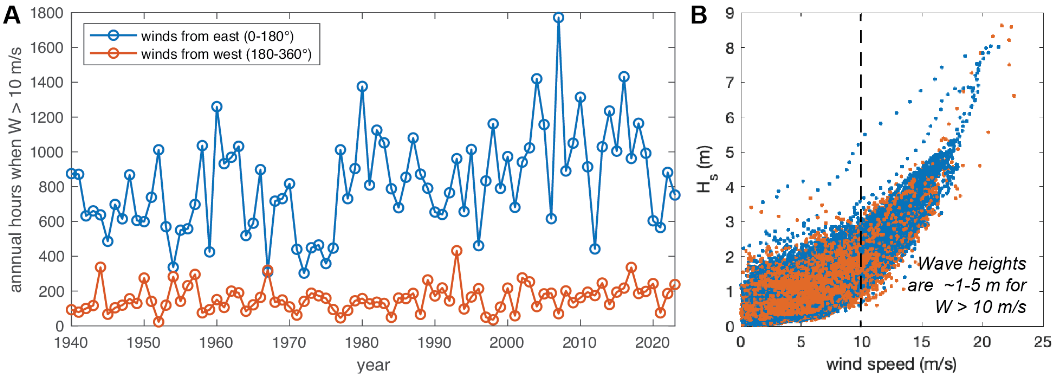

Figure 6: ERA5 wind and wave information. A) Time series of annual hours when wind speeds (W) exceeded 10 m/s for easterly winds (blue) and westerly winds (orange). B) Scatterplot of significant wave heights (for combined wind waves and swell) versus wind speeds (W) for the same time period. Note that for W>10 m/s, wave heights are typically 1-5 m.

sediment transport vectors directed southwestward, or obliquely on-shelf (Fig. 5B). The on-shelf transport generated by the August wind event dominated the signals at both sites, resulting in net landward transport during the entire mooring period (Fig. 5C).

4.3 Historical context from wind and wave hindcasts

Easterly winds have been a dominant wind pattern in the summer (and throughout the year) during the entire ∼80-year hindcast record from ERA5 (Figs. 6, C1). Wind roses from the open-water months (July, August, and September) for 1960-1979, 1980-1999, and 2000-2019 highlight a dominance of strong easterly winds (Fig. C1), in keeping with recent data (2018-2022) from Prudhoe Bay measurements and ERA5 hindcasts (Fig. 2A,B). The strongest winds during this season tend to arrive in September (Fig. C1).

When binned into two categories–winds from the east (0-180°C on the compass) and west (180-360°C on the compass)–the annual hours when winds exceed 10 m/s is ∼400-1800 for easterly winds (with a mean value 816 hrs per year; Fig. 6A). Westerly winds exceed 10 m/s for only ∼0-400 hours per year (with a mean value of 159 hrs per year).

It is worth noting that for both westerly and easterly winds, significant wave heights are well correlated, meaning stronger winds bring stronger waves (Fig. 6B). For wind speeds greater than 10 m/s, offshore wave heights (at the location where ERA5 data were queried; Appendix C) are typically 1-5 m (Fig. 6B). Wave heights do exhibit a seasonal dependence; progressively larger waves (and swell) form in August and September (Appendix

C) as a consequence of increasing fetch during the season of ice melt (e.g., Thomson et al., 2016).

5 Discussion

5.1 Winds, waves, and hydrodynamics

Harrison Bay is a shallow, low-relief, microtidal shelf where winds, waves, and coastal water-level changes dominate the hydrodynamics and resultant sediment transport. Westerly winds are routinely weaker than easterly winds (Fig. 6A), but they do drive eastward surface flows and a modest amount (∼7 cm) of coastal setup (Fig. 7A,C). Based on observed current patterns (Figs. 3, 4), setdown during westerly winds generates nearbed, off-shelf flow that could reasonably be called downwelling, in accordance with observations by Héquette & Hill (1993) during storms on the similarly shallow inner Mackenzie (Canadian Beaufort) shelf. In Harrison Bay, these downwelling events draw relatively warm, fresh water from nearshore coastal zones offshore through the boundary layer (Figs. 3E, 4B). These westerly winds also generate moderately sized waves which are bigger at T2 than T1–likely because T1 is more sheltered than T2. Combined wave-current shear stresses are modest (generally <1 cm/s at both T1B and T2B; Figs. 3I, 4F).

During easterly storm events, strong wind-driven currents destroy stratification in the water column between the surface melt layer and colder bottom layers, and bring larger waves to both transects (Figs. 3, 4). Westward surface currents are accompanied by coastal setdown, and near-bed waters flow on-shelf in the boundary layer (i.e., shallow upwelling; Fig. 7). In contrast to the downwelling flows of warmer, fresher water observed during westerly winds, these easterly winds draw cold, salty water from depth onto the middle to inner shelf (Figs. 3E, 4B). This flow pattern is not surprising in light of observations of coastal setdown and associated upwelling on the slope at sites farther west (Okkonen et al., 2009). In Harrison Bay, these events generate strong combined wave-current shear velocities of more than 1 cm/s at T1B and >3 cm/s at T2B (Figs. 3I, 4F).

It is interesting to note the frequency and strength of these upwelling and downwelling near-bed currents. In the period observed, these setup and setdown events occurred every few days (as highlighted by the mean currents; see Fig. I1 in Appendix I), and were generally accompanied by moderate to strong wave energy. However, even in the absence of waves,

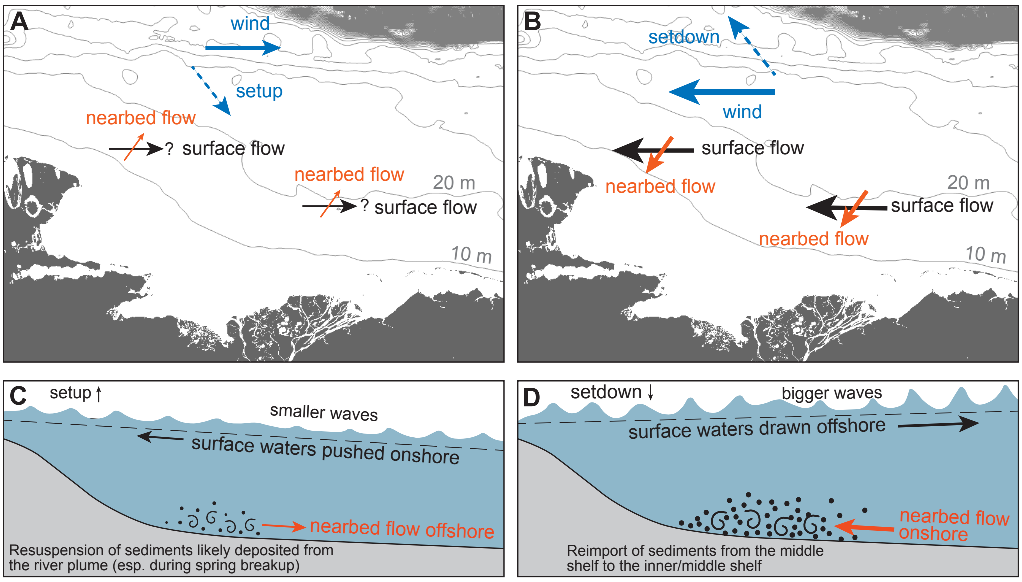

Figure 7: Conceptual diagrams of observed flow patterns and sediment transport directions for contrasting summertime wind directions. A) Nearbed and surface flow vectors for westerly winds. (Note that surface flow vectors are inferred.) B) Nearbed and surface flow vectors for easterly winds. C) Cross-shelf profile of coastal setup, relatively smaller wave heights, and nearbed seaward sediment transport associated with westerly winds in (A). D) Cross-shelf profile of coastal setdown, relatively larger wave heights, and strong nearbed landward sediment transport associated with easterly winds in (B).

the currents alone routinely produced u_* values >1 cm/s at T2B (and values of >0.5 cms/ at T1B; Fig. J1 in Appendix J).

5.2 Sediment transport - forcing mechanisms and directions

The wind- and wave-forced conditions on the shallow Beaufort Shelf create an interesting summertime convergence of sediment on the middle shelf. During westerly winds, bed stresses generated by winds and waves are sufficient to resuspended fine-grained bed sediments into the bottom boundary layer, and downwelling flows advect this material in an off-shelf direction (Fig. 7A, C). It is worth noting that this type of resuspension and transport is variable in strength, however, during different westerly wind events (e.g., Aug 7 vs Aug 12). This may be an indicator that sediment availability on the inner shelf is patchy – which would be consistent with observations of patchy mud distributions (Eidam et al., 2025).

During easterly wind events, strong winds destroy stratification, create upwelling currents, and bring large waves - all of which serve to increase near-bed shear stresses to values approaching 1.5 cm/s at T1B and 3.5 cm/s at T2B, which exceed a nominal

1 cm/s critical stress for sands (e.g., Miller et al., 1977. The resulting nearbed sediment concentrations are relatively large for a shelf environment: >100 mg/L at T1A and >500 mg/L at T2A. Because these high TSS signals peak synchronously with u_*, it seems that much of this sediment was locally resuspended, meaning it was previously stored at the "A" sites (or between the "A" and "B" sites). In other words, sediment was stored between ∼10-m and 15-m water depths (and possibly at shallower depths), despite seaward transport during the preceding westerly winds (Fig. 7B, D).

Related work from the same project showed the presence of a 1-2 cm thick layer of high-porosity, light-colored, fine-grained sediment draped over coarser and/or more compacted sediments at various sites throughout the bay (Eidam et al., 2025). It seems plausible that this layer forms as a suspension deposit during the winter and/or (more likely) during spring breakup, when muddy water from the spring Colville freshet often spreads under the ice (see Reimnitz, 2002; Cooper et al., 2024). During the summer, these sediments may provide a source of easily resuspendable material that contributes to the high concentrations observed during mooring period. It is interesting that the dominance of easterly winds and upwelling currents, however, promotes retention of these sediments on the inner shelf rather than export (see Figs. 2, 5, 6, 7).

5.3 Contextualizing inner-shelf sediment convergence in relation to other global shelf systems

The net landward transport and strong convergence of muddy sediments on the inner shelf makes the Beaufort system different from diverse other shelf systems, but not entirely unusual. On many shelves (where rivers are the dominant sediment supply), advection in river plumes, wave energy, frontal processes, downwelling currents, and gravity flows serve to export sediment out of the nearshore zone to deeper sites (e.g., Nittrouer & Wright, 1994). Terrestrially derived mud often deposits in a belt on the middle shelf – especially on high-energy or wave-dominated shelves (e.g., the Washington margin, USA, Sternberg, 1986; Waipaoa margin, New Zealand, Kuehl et al., 2016; and Iberian margin, Portugal and Spain, Dias et al., 2002). In many cases, alongshelf transport is even stronger than across-shelf transport due to prevailing currents, and so muds which are delivered to the middle shelf are also advected along-shelf to form an extensive mid-shelf "depocenter" spanning many kilometers down-drift of a fluvial source (e.g., Sternberg, 1986; Nittrouer

& Wright, 1994). In cases where wave energy is low (e.g., in a sheltered coastal setting) and/or sediment loads are quite high, muds may be found near shore (see McCave, 1972).

Episodic *on-shelf* (landward) transport of terrestrially derived muds has also been observed in some shelf settings, however (even beyond the nearshore zone where wave dynamics can drive seasonal transport of sand toward shore in many systems). In coastal Louisiana, cold fronts can generate upwelling flows which promote landward transport of fluvially derived sediments (e.g., Kineke et al., 2006). Despite the net direction of transport being off-shelf and along-shelf in this region, these episodic onshore transport events provide enough sediment to the coastal chenier plan to allow for coastal progradation (Roberts et al., 1989).

The Alaskan Beaufort Shelf is perhaps more analogous to a low-relief, fluvially dominated shelf like coastal Louisiana than to a high-relief, wave-dominated shelf where classic mid-shelf mud belts form While sediment loads from bluffs and rivers on the North Slope are much smaller than from large rivers like the Mississippi, sediments delivered to Harrison Bay are transported episodically by waves and currents during just a few months per year when sea ice has retreated. This means that the shelf may appear to be more sediment-dominated (like the Gulf Coast) than energy-dominated or wave-dominated (like the Washington, Waipaoa, and Iberian margins) because of a relative lack of energy rather than an abundant sediment supply.

The net landward transport of sediment is also an interesting phenomenon. In coastal Louisiana, landward transport events - though not the dominant signal - promote some coastal progradation. By comparison, shorelines in Harrison Bay are net erosional (Gibbs & Richmond, 2017), and in fact the inner shelf is generally erosional to depths of $\sim$12-15 m (Heath, 2024), as predicted by earlier conceptual models of shelf backstepping in response to shoreline retreat (Reimnitz et al., 1988). If sediments are generally retained on the inner shelf in summer and generally immobile in the winter, how do net export and thus net shelf erosion occur? There seem to be two possible explanations which are both related to the prevalence of autumn storms. First, strong storm energy in the fall (Fig. C1) may promote strong net off-shelf sediment transport, e.g., through wave-driven resuspension of inner-shelf muds and formation of sediment gravity flows (wave-supported fluid muds; see Traykovski et al., 2000). However, easterly storms dominate the weather patterns even in the fall (Fig. C1), and so fall storms should simply intensify inner-shelf convergence.

Furthermore, even if wave action was sufficiently strong to initiate wave-supported fluid muds, it is difficult (though not impossible) to picture these flows being sustained on the middle shelf where the bed roughness can be on the order of 1 m or more due to keel scours (see Eidam et al., 2025). The second and more plausible explanation is related to a theory by Kempema & Reimnitz (1989) that the entire annual budget of sediment supplied to the Beaufort Shelf by rivers and bluffs may in fact be removed each year by sea-ice entrainment and ice rafting. During autumn storms, strong wave energy creates strong resuspension of the sediments which were trapped on the inner shelf during summer (Fig. 8A, B). "Frazil" ice (seed ice crystals) is also generated due to the loss of heat from the ocean. Sediment resuspended from the shelf (inshore of 30 m; Reimnitz et al., 1998) then becomes trapped within a buoyant layer of frazil ice at the surface which freezes to form new sea ice (Fig. 8C, D; Kempema & Reimnitz, 1989). This ice is later rafted seaward in the spring, potentially displacing its sediment load to deeper waters if the ice is rafted off-shelf before completely melting (Barnes et al., 1982). While only limited data exist about sediment budgets in sea ice, the present study suggests that summertime wind and wave dynamics create ideal conditions to focus sediment in the zone where new, muddy ice is likely to form–thus enhancing off-shelf export, rather than promoting on-shelf trapping. If true, then this finding would help validate earlier predictions (Kempema & Reimnitz, 1989; Barnes et al., 1982) that ice can remove most of the annual sediment derived from bluffs and rivers – and would help explain the lack of coastal progradation in conjunction with landward shelf sediment flux in the summer.

5.4 Comparisons to other Arctic shelf systems

On the shallow and extremely wide Laptev Shelf, landward transport of sediment has also been observed during the summer – but as a result of estuarine-like circulation that is created under the large, seaward-flowing Laptev River plume (Wegner et al., 2005). Despite the different hydrodynamics, the net result of mid-shelf sediment trapping is similar to what has been observed here for Harrison Bay. Interestingly, convergence on the Laptev shelf is further enhanced by sediment resuspension and landward flux when polynyas (gaps in the ice) form during winter storms (Wegner et al., 2005).

Evidence from the Canadian Beaufort Sea confirms that wind-driven dynamics are key to cross-shelf sediment flux, but suggests that dominant wind direction may be a major control on net storage or export of sediment from the shelf, at least in the summer months.

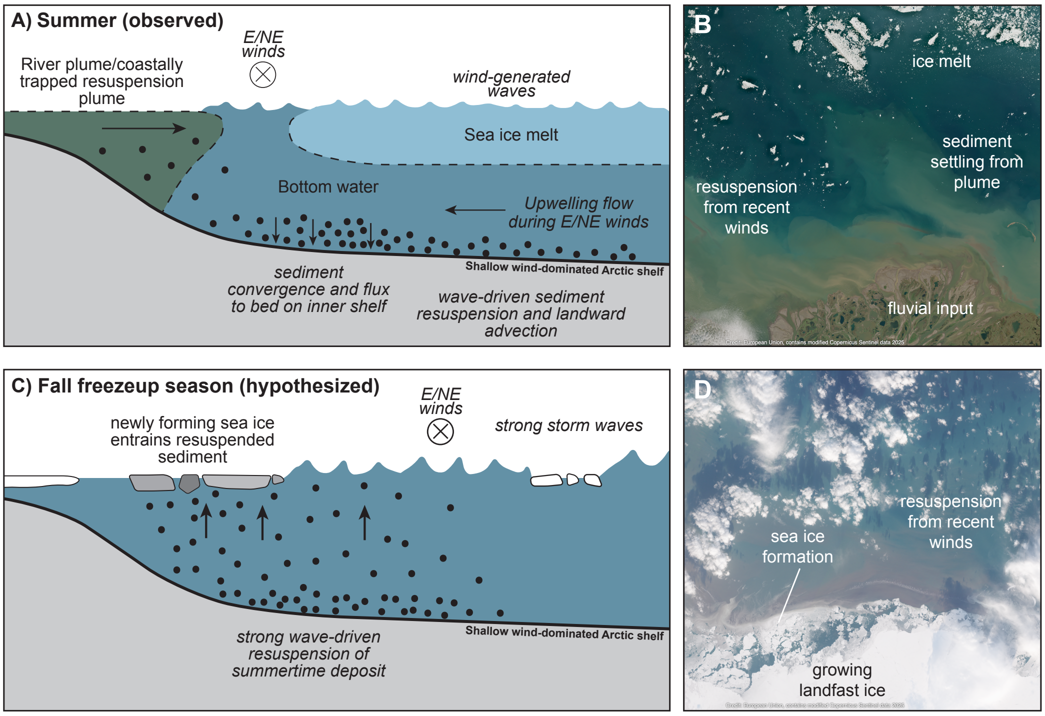

Figure 8: Conceptual diagram of observed summertime and hypothesized freezeup-season sediment dynamics. A) During the summer, E/NE winds generate waves and upwelling, which together serve to resuspend and advect sediment in a generally landward direction. This sediment converges with settling coastal plume sediment on the inner shelf to form an ephemeral deposit. B) During the freezeup season, strong storms resuspend this ephemeral deposit, making sediments available in suspension to be incorporated into newly forming sea ice (typically together with frazil ice).

Near the Mackenzie River, northwesterly storms dominate the wind patterns, and create coastal setup – especially where the shoreline is backed by bluffs rather than barrier islands (barrier islands allow spillover and reduce the strength of the setup; Héquette & Hill, 1993; Lintern et al., 2013). These storms also bring waves, and the combination of wave-driven resuspension and ~0.5-m/s downwelling currents is thought to accomplish seaward sediment dispersal, though direct measurements were not available (Héquette & Hill, 1993).

The results of this study can thus be paired with work from the Laptev Sea Shelf and Canadian Beaufort/Mackenzie shelf to provide a picture of three styles of Arctic cross-shelf sediment dispersal:

- Canadian Beaufort Shelf: Northwesterly storms are dominant and create setup (especially where bluffs rather than barrier islands border the shelf; waves and strong downwelling flows accomplish seaward sediment dispersal (Héquette & Hill, 1993);

- Alaskan Beaufort Shelf: Easterly storms dominate, and create setdown; waves and strong upwelling flows focus sediments that previously settled from suspension (likely during spring breakup) onto the inner shelf (inshore of the 15-m isobath) – but this simply makes them more available for sea-ice entrainment during fall storms (*this study*);
- Laptev Sea Shelf: The Laptev River plume creates estuarine-like circulation on the shelf which advects sediments settling from the plume landward to become trapped on the shelf; landward transport also occurs during winter polynya events (Wegner et al., 2005). Summertime plume (and thus sediment transport) can vary in response to natural inter-annual variability in atmospheric forcing, however (Wegner et al., 2013).

5.5 Historical context and future implications

The mooring observations collected in this study span just one month. Are they representative of conditions throughout the open-water season? The answer is likely yes, because easterly wind events dominate both in summer months as well as throughout the entire year, based on many decades of climate reanalaysis data (Figs. 6, C1). One caveat to this interpretation is the potential occurrence of gravity flows, which would be an interesting problem to model since the keel scours present extremely large-scale bed roughness elements. Absent gravity flows, it seems plausible that during any given summer, sediments will be routinely focused on the inner shelf.

How would the sedimentary regime change in the future if sea ice stopped forming but the wave climate increased? Storms are often cited as a mechanism which exacerbates coastal erosion, not least because rapid erosion has been documented during extreme storm events (waves cause mechanical erosion of permafrost-rich bluffs). However, on the Beaufort Shelf, stronger waves may simply lead to more inner-shelf sediment storage if easterly winds continue to dominate the weather patterns. This may in fact already be happening based on evidence of an increasing number of upwelling events on the outer shelf each year (see Pickart, Schulze, et al., 2013). If there is then no sea ice to remove this sediment, inner shelf erosion may be slowed and new coastal landforms may even develop.

6 Conclusions

Net summertime sediment transport on the Alaskan Beaufort Shelf is regulated by easterly wind events which bring strong wave energy and upwelling flows. Waves resuspend sediments and the upwelling flows advect them landward, where they form an ephemeral summertime deposit on the inner shelf. Based on past measurements and predictions (Reimnitz et al., 1998; Kempema & Reimnitz, 1989; Barnes et al., 1982), it seems likely that this material is then resuspended by waves during fall storms and entrained into newly forming sea ice, some of which is rafted elsewhere during spring breakup. The wind- and wave-driven convergence of sediment on the inner shelf thus seems to be a key mechanism for *off-shelf* transport – rather than the formation of a shelf depocenter – because it makes sediment more readily available for sea-ice entrainment in the fall. The processes of up-slope sediment transport during the summer (observed in this study) and off-shelf export by ice (observed in other studies) set this system apart from lower-latitude systems where net transport is generally seaward. It is worth noting that in some lower-latitude coastal systems, on-shelf transport does occur – e.g., in coastal Louisiana, where upwelling conditions are occasionally created and lead to shoreline progradation through chenier plains (Kineke et al., 2006; Roberts et al., 1989). By analogy, if prevailing easterly winds remained the norm but sea ice disappeared and wave energy increased, the Alaskan Beaufort Shelf could potentially see an increase in sediment retention on the shelf (due to increased sediment convergence and a lack of ice entrainment and rafting to remove it). Could the system then develop prograding coastlines similar to some Gulf Coast regions? This is an interesting system to watch in light of predictions of sea-ice losses in the coming decades (e.g., Jahn et al., 2024).

Within the context of pan-Arctic shelves, the Alaska Beaufort Shelf offers an example of strong summertime sediment convergence on the shelf - but other shelves seem to experience different sediment dispersal pathways. The Canadian Beaufort Shelf is dominated by northwesterly rather than easterly winds (Héquette & Hill, 1993), and thus strong off-shelf transport may dominate in contrast to the sediment convergence observed in the Alaskan Beaufort sector. On the Laptev Sea Shelf, which is a much wider shelf with stronger river influence, the Laptev River plume creates estuarine-like circulation which, together with wintertime polynyas, focuses sediment on the inner shelf (Wegner et al., 2005). These mechanisms of sediment focusing may make sediment more readily available for fall-season ice entrainment, as in the case of Harrison Bay–but for different reasons. Evaluating the storage, export, and erosion of sediments (and related nutrients and pollutants) from Arctic shelves thus requires careful consideration of summertime wind and wave dynamics, and consideration of whether sediments are converging or diverging prior to winter storms and ice formation.

Data Availability

Mooring data presented here were submitted to the Arctic Data Center in February 2025 and are pending publication under identifier urn:uuid:c48426fe-c2f5-454c-aa97-9380836bd4c2 (the dataset is entitled 'Mooring data from Harrison Bay, Alaska, August-September 2022'). Mooring data from the CODA project are available at `https://arcticdata.io/catalog/view/doi:10.18739/A2DF6K45W`.

Acknowledgments

The field portion of this project was funded by NSF grants OPP 1913195 (Eidam) and OPP 1912836 (co-PI N. Stark). Analysis and writing were supported by Oregon State University. The author thanks Dr. Nick Brilli, Dan Duncan, Mike Fleming (*R/V Ukpik*), Caroline Cooper, Dr. Jaap Nienhuis, Dr. Nina Stark, Adrian Heath, Emily Iseley, Stephanie Fisher, and Dr. Jeremy Kasper for their support of mooring deployments and field studies; and Drs. Jim Thomson, Steve Dykstra, and Harvey Seim for helpful discussions about wind dynamics.

References note for draft version of paper

Please note that in my version of latex, many of the citations do not include correct capitalization of paper titles. These will be corrected when typeset should the paper be published.

References

Aagaard, K. (1984). The beaufort undercurrent. In *The alaskan beaufort sea* (pp. 47–71). Elsevier.

Arnborg, L., Walker, H. J., & Peippo, J. (1967). Suspended load in the Colville River, alaska, 1962. *Geografiska Annaler: Series A, Physical Geography*, *49*(2-4), 131–144.

Barnes, P. W., Rearic, D. M., & Reimnitz, E. (1984). Ice gouging characteristics and processes. In *The Alaskan Beaufort Sea* (pp. 185–212). Elsevier.

Retrieved 2024-01-24, from https://linkinghub.elsevier.com/retrieve/pii/B9780120790302500150 doi: 10.1016/B978-0-12-079030-2.50015-0

Barnes, P. W., Reimnitz, E., & Fox, D. (1982). Ice rafting of fine-grained sediment, a sorting and transport mechanism, beaufort sea, alaska. *Journal of Sedimentary Research*, *52*(2), 493–502.

Barnes, P. W., & Reiss, T. E. (1983). *Erosion and migration of an artificial sand and gravel island, Niakuk III, Beaufort Sea, Alaska* (Tech. Rep.). US Geological Survey,.

Boudreau, B. P., & Hill, P. S. (2020). Rouse revisited: the bottom boundary condition for suspended sediment profiles. *Marine Geology*, *419*, 106066.

Brilli, N. (2022). *Influence of Geotechnical Properties on Sediment Dynamics, Erodibility, and Geomorphodynamics in Coastal Environments Based on Field Measurements* (Doctoral dissertation, Virginia Tech). Retrieved https://vtechworks.lib.vt.edu/items/266adfc4-2cc6-4c9d-baf0-9cdeabd4bd27, from https://vtechworks.lib.vt.edu/items/266adfc4-2cc6-4c9d-baf0-9cdeabd4bd27

Cooper, C., Eidam, E., Seim, H., & Nienhuis, J. (2024). Effects of sea ice on arctic delta evolution: A modeling study of the colville river delta, alaska. *Journal of Geophysical Research: Earth Surface*, *129*(9), e2024JF007742.

Dias, J., Jouanneau, J., Gonzalez, R., Araújo, M., Drago, T., Garcia, C., ... Weber, O. (2002). Present day sedimentary processes on the northern iberian shelf. *Progress in Oceanography*, *52*(2-4), 249–259.

Doxaran, D., Devred, E., & Babin, M. (2015, June). A 50 % increase in the mass of terrestrial particles delivered by the Mackenzie River into the Beaufort Sea (Canadian Arctic Ocean) over the last 10 years. *Biogeosciences*, *12*(11), 3551–3565. Retrieved 2024-01-24, from https://bg.copernicus.org/articles/12/3551/2015/ doi: 10.5194/bg-12-3551-2015

Eidam, E., Brilli, N., Heath, A., Cooper, C., Duncan, D., Nienhuis, J., & Stark, N. (2022). Morphology and sediments of the subaqueous colville river delta (alaska). In *Agu fall meeting abstracts* (Vol. 2022, pp. OS25D–0953).

Eidam, E., Cooper, C., Heath, A., Nienhuis, J., & Seim, H. (2023). Summertime sediment-transport dynamics on an arctic continental shelf. *AGU23*.

Eidam, E., Stark, N., Nienhuis, J. H., Duncan, D., Brilli, N., Kallioras, N., ...

Heath, A. (2025). Seafloor sediments, morphologic features, and geotechnical properties of harrison bay in the alaskan beaufort sea. *Authorea Preprints*.

Eidam, E., Thomson, J., Malito, J., & Hosekova, L. (2023). Morphology and sediment dynamics of blossom shoals at icy cape, alaska. *Authorea Preprints*.

Farquharson, L., Mann, D. H., Grosse, G., Jones, B. M., & Romanovsky, V. (2016). Spatial distribution of thermokarst terrain in arctic alaska. *Geomorphology*, *273*, 116–133.

Feng, D., Gleason, C. J., Lin, P., Yang, X., Pan, M., & Ishitsuka, Y. (2021, November). Recent changes to Arctic river discharge. *Nature Communications*, *12*(1), 6917. Retrieved 2024-01-24, from `https://www.nature.com/articles/s41467-021-27228-1` doi: 10.1038/s41467-021-27228-1

Foukal, N. P., Pickart, R. S., Moore, G., & Lin, P. (2019). Shelfbreak downwelling in the alaskan beaufort sea. *Journal of Geophysical Research: Oceans*, *124*(10), 7201–7225.

Gibbs, A. E., Nolan, M., Richmond, B. M., Snyder, A. G., & Erikson, L. H. (2019, July). Assessing patterns of annual change to permafrost bluffs along the North Slope coast of Alaska using high-resolution imagery and elevation models. *Geomorphology*, *336*, 152–164. Retrieved 2024-01-24, from `https://linkinghub.elsevier.com/retrieve/pii/S0169555X19301278` doi: 10.1016/j.geomorph.2019.03.029

Gibbs, A. E., & Richmond, B. M. (2017). *National assessment of shoreline change—summary statistics for updated vector shorelines and associated shoreline change data for the north coast of Alaska, US-Canadian Border to Icy Cape* (Tech. Rep.). US Geological Survey.

Harris, P. T., & Macmillan-Lawler, M. (2016). Global overview of continental shelf geomorphology based on the srtm30_plus 30-arc second database. *Seafloor mapping along continental shelves: Research and techniques for visualizing benthic environments*, 169–190.

Heath, A. (2024). Sedimentation and erosion on an arctic continental shelf: Harrison bay and colville river delta, alaska. *Thesis, Oregon State University*.

Heath, A., Eidam, E., & Cooper, C. (2024). *Sediment deposition on the Alaskan Beaufort Shelf: a geochronology study in a changing Arctic environment.* Retrieved from `https://agu.confex.com/agu/OSM24/meetingapp.cgi/Paper/1490619`

(Ocean Sciences Meeting)

Hequette, A., & Aernouts, D. (2010, July). The influence of nearshore sand bank dynamics on shoreline evolution in a macrotidal coastal environment, Calais, northern France. *Continental Shelf Research*, *30*(12), 1349–1361. Retrieved 2021-01-26, from https://linkinghub.elsevier.com/retrieve/pii/S0278434310001561 doi: 10.1016/j.csr.2010.04.017

Herman, Y. (1974). *Marine geology and oceanography of the arctic seas.* Springer Science & Business Media.

Hersbach, H., Bell, B., Berrisford, P., Biavati, G., Horányi, A., Muñoz Sabater, J., ... Thépaut, J.-N. (2023). *ERA5 hourly data on single levels from 1940 to present.* Copernicus Climate Change Service (C3S) Climate Data Store (CDS). doi: 10.24381/cds.adbb2d47

Hill, P. R., Blasco, S. M., Harper, J. R., & Fissel, D. B. (1991, August). Sedimentation on the Canadian Beaufort Shelf. *Continental Shelf Research*, *11*(8-10), 821–842. Retrieved 2024-01-24, from https://linkinghub.elsevier.com/retrieve/pii/027843439190081G doi: 10.1016/0278-4343(91)90081-G

Hill, P. S., Fox, J. M., Crockett, J. S., Curran, K. J., Friedrichs, C. T., Geyer, W. R., ... others (2007). Sediment delivery to the seabed on continental margins. *Continental Margin Sedimentation: From Sediment Transport to Sequence Stratigraphy*, 49–99.

Holmes, R. M., McClelland, J. W., Peterson, B. J., Shiklomanov, I. A., Shiklomanov, A. I., Zhulidov, A. V., ... Bobrovitskaya, N. N. (2002, December). A circumpolar perspective on fluvial sediment flux to the Arctic ocean. *Global Biogeochemical Cycles*, *16*(4). Retrieved 2024-01-24, from https://agupubs.onlinelibrary.wiley.com/doi/10.1029/2001GB001849 doi: 10.1029/2001GB001849

Hošeková, L., Eidam, E., Panteleev, G., Rainville, L., Rogers, W. E., & Thomson, J. (2021). Landfast ice and coastal wave exposure in northern Alaska. *Geophysical Research Letters*, *48*(22), e2021GL095103.

Héquette, A., & Hill, P. R. (1993, August). Storm-generated currents and offshore sediment transport on a sandy shoreface, Tibjak Beach, Canadian Beaufort Sea. *Marine Geology*, *113*(3-4), 283–304. Retrieved 2024-01-24, from https://linkinghub.elsevier.com/retrieve/pii/002532279390023O doi:

10.1016/0025-3227(93)90023-O

Jahn, A., Holland, M. M., & Kay, J. E. (2024). Projections of an ice-free arctic ocean. *Nature Reviews Earth & Environment*, *5*(3), 164–176.

Jakobsson, M., Grantz, A., Kristoffersen, Y., & Macnab, R. (2003). Physiographic provinces of the arctic ocean seafloor. *Geological Society of America Bulletin*, *115*(12), 1443–1455.

Jones, B. M., Arp, C. D., Jorgenson, M. T., Hinkel, K. M., Schmutz, J. A., & Flint, P. L. (2009). Increase in the rate and uniformity of coastline erosion in arctic alaska. *Geophysical Research Letters*, *36*(3).

Kempema, E., & Reimnitz, E. (1989). Sea Ice Sediment Entrainment and Rafting in the Arctic. *SEPM Journal of Sedimentary Research*, *Vol. 59*. Retrieved 2024-01-24, from `https://pubs.geoscienceworld.org/jsedres/article/59/2/308-317/113821` doi: 10.1306/212F8F80-2B24-11D7-8648000102C1865D

Kineke, G., Higgins, E., Hart, K., & Velasco, D. (2006). Fine-sediment transport associated with cold-front passages on the shallow shelf, gulf of mexico. *Continental Shelf Research*, *26*(17-18), 2073–2091.

Kovacs, A., & Mellor, M. (1974). Sea ice morphology and ice as a geologic agent in the southern Beaufort Sea. *In: The coast and shelf of the Beaufort Sea*.

Kuehl, S. A., Alexander, C. R., Blair, N. E., Harris, C. K., Marsaglia, K. M., Ogston, A. S., ... others (2016). A source-to-sink perspective of the waipaoa river margin. *Earth-Science Reviews*, *153*, 301–334.

Lantuit, H., Overduin, P. P., Couture, N., Wetterich, S., Aré, F., Atkinson, D., ... Vasiliev, A. (2012, March). The Arctic Coastal Dynamics Database: A New Classification Scheme and Statistics on Arctic Permafrost Coastlines. *Estuaries and Coasts*, *35*(2), 383–400. Retrieved 2024-01-24, from `http://link.springer.com/10.1007/s12237-010-9362-6` doi: 10.1007/s12237-010-9362-6

Lintern, D. G., Macdonald, R. W., Solomon, S. M., & Jakes, H. (2013, November). Beaufort Sea storm and resuspension modeling. *Journal of Marine Systems*, *127*, 14–25. Retrieved 2024-01-24, from `https://linkinghub.elsevier.com/retrieve/pii/S092479631100282X` doi: 10.1016/j.jmarsys.2011.11.015

Macdonald, R., Solomon, S., Cranston, R., Welch, H., Yunker, M., & Gobeil, C. (1998, January). A sediment and organic carbon budget for the Canadian Beaufort Shelf. *Marine Geology*, *144*(4), 255–273. Retrieved 2024-01-24, from https://linkinghub.elsevier.com/retrieve/pii/S0025322797001060 doi: 10.1016/S0025-3227(97)00106-0

McCave, I. (1972). Transport and escape of fine-grained sediment from shelf areas. *Shelf sediment transport: process and pattern*, 225–248.

Miller, M., McCave, I., & Komar, P. (1977). Threshold of sediment motion under unidirectional currents. *Sedimentology*, *24*(4), 507–527.

Milliman, J. D., & Meade, R. H. (1983). World-wide delivery of river sediment to the oceans. *The Journal of Geology*, *91*(1), 1–21.

Naidu, A. S., & Mowatt, T. C. (1983). Sources and dispersal patterns of clay minerals in surface sediments from the continental-shelf areas off Alaska. *Geological Society of America Bulletin*, *94*(7), 841. Retrieved 2024-01-24, from https://pubs.geoscienceworld.org/gsabulletin/article/94/7/841-854/202863 doi: 10.1130/0016-7606(1983)94⟨841:SADPOC⟩2.0.CO;2

NBDC. (2025). *Station prda2 - 9497645 - prudhoe bay, ak* (Dataset). National Buoy Data Center; National Oceanic and Atmospheric Administration. (url https://www.ndbc.noaa.gov/station$_{p}age.php?station = prda2$)

Nielsen, D. M., Pieper, P., Barkhordarian, A., Overduin, P., Ilyina, T., Brovkin, V., . . . Dobrynin, M. (2022). Increase in arctic coastal erosion and its sensitivity to warming in the twenty-first century. *Nature Climate Change*, *12*(3), 263–270.

Nittrouer, C. A., & Wright, L. D. (1994). Transport of particles across continental shelves. *Reviews of Geophysics*, *32*(1), 85–113.

Okkonen, S. R. (2016). *Sea level measurements along the alaskan chukchi and beaufort coasts.* Coastal Marine Institute, University of Alaska Fairbanks.

Okkonen, S. R., Ashjian, C. J., Campbell, R. G., Maslowski, W., Clement-Kinney, J. L., & Potter, R. (2009, January). Intrusion of warm Bering/Chukchi waters onto the shelf in the western Beaufort Sea. *Journal of Geophysical Research: Oceans*, *114*(C1), 2008JC004870. Retrieved 2024-01-24, from https://agupubs.onlinelibrary.wiley.com/doi/10.1029/2008JC004870 doi: 10.1029/2008JC004870

Okkonen, S. R., & Laney, S. R. (2021, December). Optical, Structural and Kinematic Characteristics of Freshwater Plumes Under Landfast Sea Ice During the Spring Freshet in the Alaskan Coastal Arctic. *Journal of Geophysical Research: Oceans*, *126*(12), e2021JC017549. Retrieved 2024-01-24, from https://agupubs.onlinelibrary.wiley.com/doi/10.1029/2021JC017549 doi: 10.1029/2021JC017549

Perovich, D. K., & Richter-Menge, J. A. (2009). Loss of sea ice in the arctic. *Annual review of marine science*, *1*(1), 417–441.

Pickart, R. S. (2004). Shelfbreak circulation in the alaskan beaufort sea: Mean structure and variability. *Journal of Geophysical Research: Oceans*, *109*(C4).

Pickart, R. S., Schulze, L. M., Moore, G., Charette, M. A., Arrigo, K. R., van Dijken, G., & Danielson, S. L. (2013). Long-term trends of upwelling and impacts on primary productivity in the alaskan beaufort sea. *Deep Sea Research Part I: Oceanographic Research Papers*, *79*, 106–121.

Pickart, R. S., Spall, M. A., & Mathis, J. T. (2013). Dynamics of upwelling in the alaskan beaufort sea and associated shelf–basin fluxes. *Deep Sea Research Part I: Oceanographic Research Papers*, *76*, 35–51.

Piliouras, A., Jones, B. M., Clevenger, T., Gibbs, A. E., & Rowland, J. C. (2023). Variability in terrestrial characteristics and erosion rates on the alaskan beaufort sea coast. *Environmental Research Letters*, *18*(11), 114050.

Pond, S., & Pickard, G. (1983). *Introductory dynamical oceanography.* Pergamon Press Ltd.

Rachold, V., Grigoriev, M. N., Are, F. E., Solomon, S., Reimnitz, E., Kassens, H., & Antonow, M. (2000, December). Coastal erosion vs riverine sediment discharge in the Arctic Shelf seas. *International Journal of Earth Sciences*, *89*(3), 450–460. Retrieved 2024-01-24, from http://link.springer.com/10.1007/s005310000113 doi: 10.1007/s005310000113

Rantanen, M., Karpechko, A. Y., Lipponen, A., Nordling, K., Hyvärinen, O., Ruosteenoja, K., ... Laaksonen, A. (2022). The arctic has warmed nearly four times faster than the globe since 1979. *Communications earth & environment*, *3*(1), 168.

Rearic, D. M. (1982). *Temporal and spatial character of newly formed ice gouges in eastern Harrison Bay, Alaska, 1977-1982* (Tech. Rep.). US Geological Survey,.

Reimnitz, E. (2002). Interaction of river discharge with sea ice in proximity of Arctic deltas: a review. *Polarforschung*, *70*, 123–134.

Reimnitz, E., & Bruder, K. F. (1972). River discharge into an ice-covered ocean and related sediment dispersal, Beaufort Sea, coast of Alaska. *Geological Society of*

America Bulletin, *83*(3), 861–866.

Reimnitz, E., Graves, S., & Barnes, P. (1988). *Beaufort Sea coastal erosion, sediment flux, shoreline evolution, and the erosional shelf profile* (Tech. Rep.). Retrieved 2024-01-24, from `https://pubs.usgs.gov/publication/i1182G` doi: 10.3133/i1182G

Reimnitz, E., & Kempema, E. W. (1982). HIGH RATES OF BEDLOAD TRANSPORT MEASURED FROM INFILLING RATE OF LARGE STRUDEL-SCOUR CRATERS IN THE BEAUFORT SEA, ALASKA.

Reimnitz, E., Maurer, D., Barnes, P., & Toimil, L. (1977). *Some physical properties of shelf surface sediments, Beaufort Sea, Alaska* (Tech. Rep.). US Geological Survey,.

Reimnitz, E., McCormick, M., Bischof, J., & Darby, D. (1998). Comparing sea-ice sediment load with beaufort sea shelf deposits; is entrainment selective? *Journal of Sedimentary Research*, *68*(5), 777–787.

Roberts, H. H., Huh, O. K., Hsu, S., Rouse Jr, L. J., & Rickman, D. A. (1989). Winter storm impacts on the chenier plain coast of southwestern louisiana.

Rudels, B., & Carmack, E. (2022). Arctic ocean water mass structure and circulation. *Oceanography*, *35*(3/4), 52–65.

Schulze, L. M., & Pickart, R. S. (2012). Seasonal variation of upwelling in the alaskan beaufort sea: Impact of sea ice cover. *Journal of Geophysical Research: Oceans*, *117*(C6).

Simpson, J. H., & Sharples, J. (2012). *Introduction to the physical and biological oceanography of shelf seas*. Cambridge University Press.

Soulsby, R. (1987). Calculating bottom orbital velocity beneath waves. *Coastal Engineering*, *11*(4), 371–380.

Soulsby, R. (1997). Dynamics of marine sands: a manual for practical applications. *Oceanographic Literature Review*, *9*(44), 947.

Sternberg, R. (1986). Transport and accumulation of river-derived sediment on the washington continental shelf, usa. *Journal of the Geological Society*, *143*(6), 945–956.

Syvitski, J. P. (2002). Sediment discharge variability in arctic rivers: implications for a warmer future. *Polar Research*, *21*(2), 323–330.

Syvitski, J. P., & Morehead, M. D. (1999). Estimating river-sediment discharge to the ocean: application to the eel margin, northern california. *Marine Geology*, *154*(1-4), 13–28.

Syvitski, J. P., Peckham, S. D., Hilberman, R., & Mulder, T. (2003). Predicting the terrestrial flux of sediment to the global ocean: a planetary perspective. *Sedimentary Geology*, *162*(1-2), 5–24.

Thomson, J., Fan, Y., Stammerjohn, S., Stopa, J., Rogers, W. E., Girard-Ardhuin, F., ... Bidlot, J.-R. (2016, September). Emerging trends in the sea state of the Beaufort and Chukchi seas. *Ocean Modelling*, *105*, 1–12. Retrieved 2024-01-24, from https://linkinghub.elsevier.com/retrieve/pii/S1463500316300622 doi: 10.1016/j.ocemod.2016.02.009

Traykovski, P., Geyer, W. R., Irish, J., & Lynch, J. (2000). The role of wave-induced density-driven fluid mud flows for cross-shelf transport on the eel river continental shelf. *Continental shelf research*, *20*(16), 2113–2140.

USGS, U. S. G. S. (2025). *Colville r at umiat ak - 15875000.* https://waterdata.usgs.gov/monitoring-location/15875000/#dataTypeId=continuous-00065-1922206742&period=P7D&showMedian=false. (Accessed: 2025 Jan 22)

Wegner, C., Bauch, D., Hölemann, J. A., Janout, M. A., Heim, B., Novikhin, A., ... Timokhov, L. (2013, February). Interannual variability of surface and bottom sediment transport on the Laptev Sea shelf during summer. *Biogeosciences*, *10*(2), 1117–1129. Retrieved 2024-01-24, from https://bg.copernicus.org/articles/10/1117/2013/ doi: 10.5194/bg-10-1117-2013

Wegner, C., Holemann, J., Dmitrenko, I., Kirillov, S., & Kassens, H. (2005, September). Seasonal variations in Arctic sediment dynamics—evidence from 1-year records in the Laptev Sea (Siberian Arctic). *Global and Planetary Change*, *48*(1-3), 126–140. Retrieved 2024-01-24, from https://linkinghub.elsevier.com/retrieve/pii/S0921818105000627 doi: 10.1016/j.gloplacha.2004.12.009

Weingartner, T. J., Danielson, S. L., Potter, R. A., Trefry, J. H., Mahoney, A., Savoie, M., ... Sousa, L. (2017, September). Circulation and water properties in the landfast ice zone of the Alaskan Beaufort Sea. *Continental Shelf Research*, *148*, 185–198. Retrieved 2024-01-24, from https://linkinghub.elsevier.com/retrieve/pii/S0278434317301590 doi: 10.1016/j.csr.2017.09.001

Wiberg, P. L., & Sherwood, C. R. (2008). Calculating wave-generated bottom orbital velocities from surface-wave parameters. *Computers & Geosciences*, *34* (10), 1243–1262.

Zimmermann, M., Erikson, L. H., Gibbs, A. E., Prescott, M. M., Escarzaga, S. M., Tweedie, C. E., ... Duvoy, P. X. (2022, June). Nearshore bathymetric changes along the Alaska Beaufort Sea coast and possible physical drivers. *Continental Shelf Research*, *242*, 104745. Retrieved 2024-01-24, from `https://linkinghub.elsevier.com/retrieve/pii/S0278434322000991` doi: 10.1016/j.csr.2022.104745

Appendix A Fluvial discharge and sediment-flux data

In order to lend context to the mooring data, the sediment flux from the Colville River was estimated based on USGS discharge data. Discharge data was obtained from the USGS gauge at Umiat which is more than 150 km upstream (USGS, 2025). Corresponding suspended sediment concentrations were computed from a rating curve which Cooper et al. (2024) calculated from data provided in Arnborg et al. (1967). While these data are quite old, they are some of the best available in situ data concerning suspended-sediment concentrations at moderate to high discharges. The sediment flux was then calculated as the product of the river discharge and suspended-sediment concentrations.

Appendix B Wind data

Wind data were obtained from National Weather Service station PRDA2 located at Prudhoe Bay (NBDC, 2025). Wind stress was calculated as follows:

$$\tau_w = C_d \rho_a W(W - u_s) \approx C_d \rho_a W^2 \tag{B1}$$

where τ_w is the wind stress (Pa, or N/m^2), C_d is a drag coefficient, ρ_a is the air density, W is the wind speed, and u_s is the surface current speed aligned with the wind. If the surface current speed is relatively small, which is a fair assumption in this environment, it can be neglected as shown above (Simpson & Sharples, 2012). The drag coefficient was computed as follows:

$$C_d = (0.63 + 0.066W \times 10^{-3}) \tag{B2}$$

though it is worth noting that a value of C_d equal to $1.4x10^{-3}$ is also a reasonable assumption (Pond & Pickard, 1983).

Appendix C Wind and wave climatologies from ERA5 output

ERA5 data were downloaded and processed as outlined in the Methods section. Fig. C1 illustrates the summertime/open-water season wind roses for three 20-year periods (1960s-1970s, 1980s-1990s, and 2000s-2010s). During the open-water season, the strongest winds generally occur in September. It is difficult to discern any strengthening in wind through time.

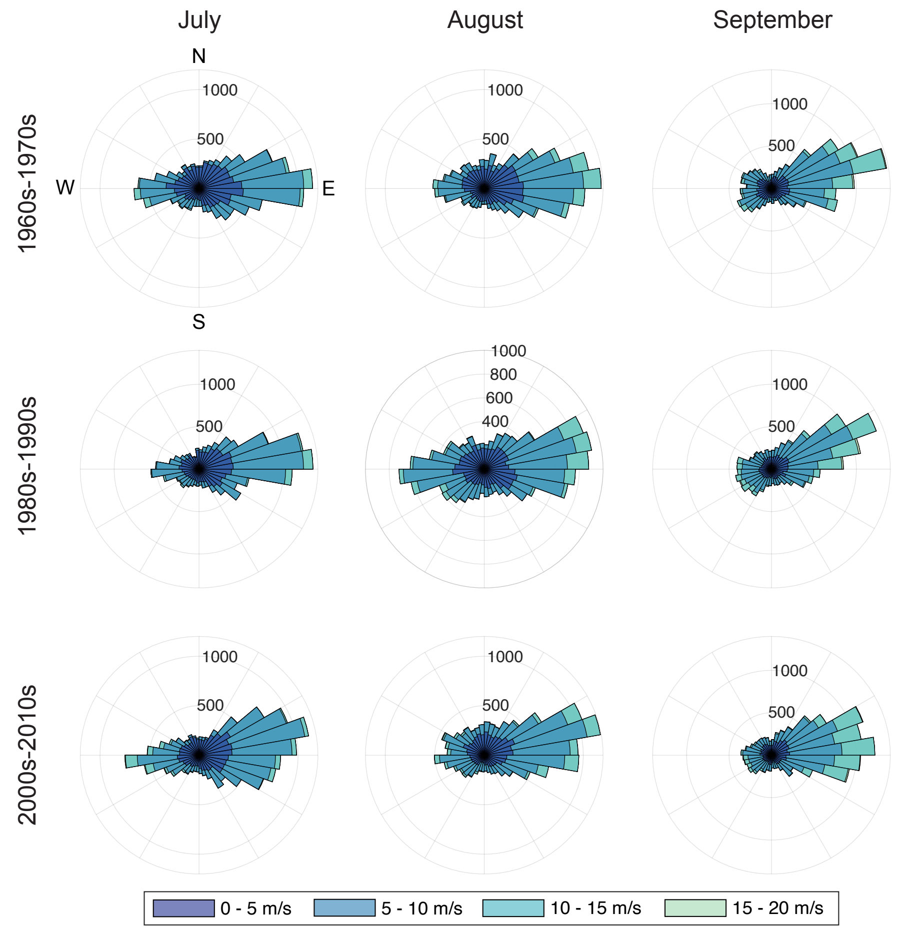

Figure C1: Wind roses by month and 20-yr period (from ERA5

Histograms of significant wave heights for wind waves and swell are provided in Figs. C2 and C3, respectively. Wind wave and swell heights both tend to increase throughout the summer, and heights have increased throughout the decades as well (as noted by others; e.g., Thomson et al., 2016).

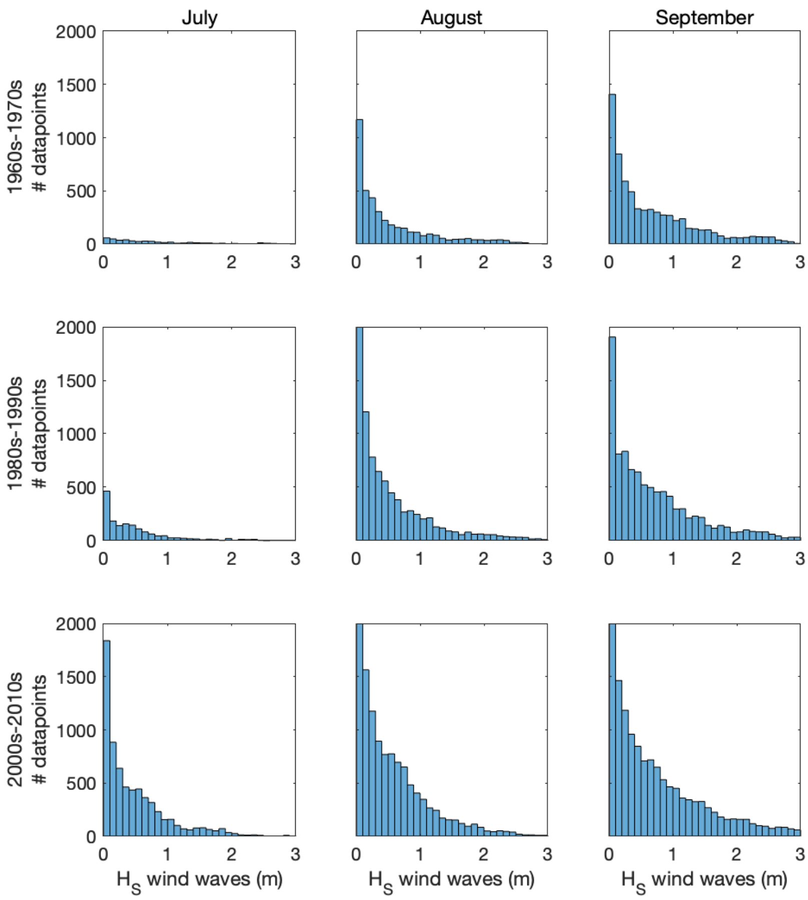

Figure C2: Histograms of significant wave heights (for wind waves) during summer months. Data are subdivided by 20-year periods.

As is expected, wave heights are correlated with wind speeds. In Fig. C4, significant heights of combined wind waves and swell show strong correlation to wind speed during the open-water season.

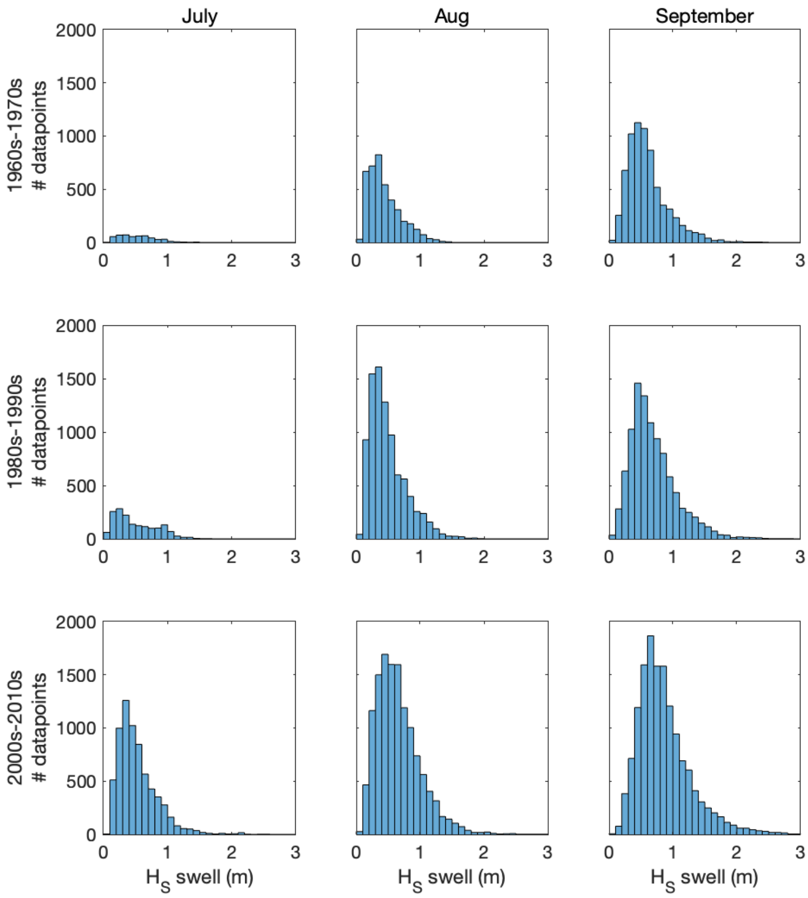

Figure C3: Histograms of significant wave heights (for swell) during summer months. Data are subdivided by 20-year periods.

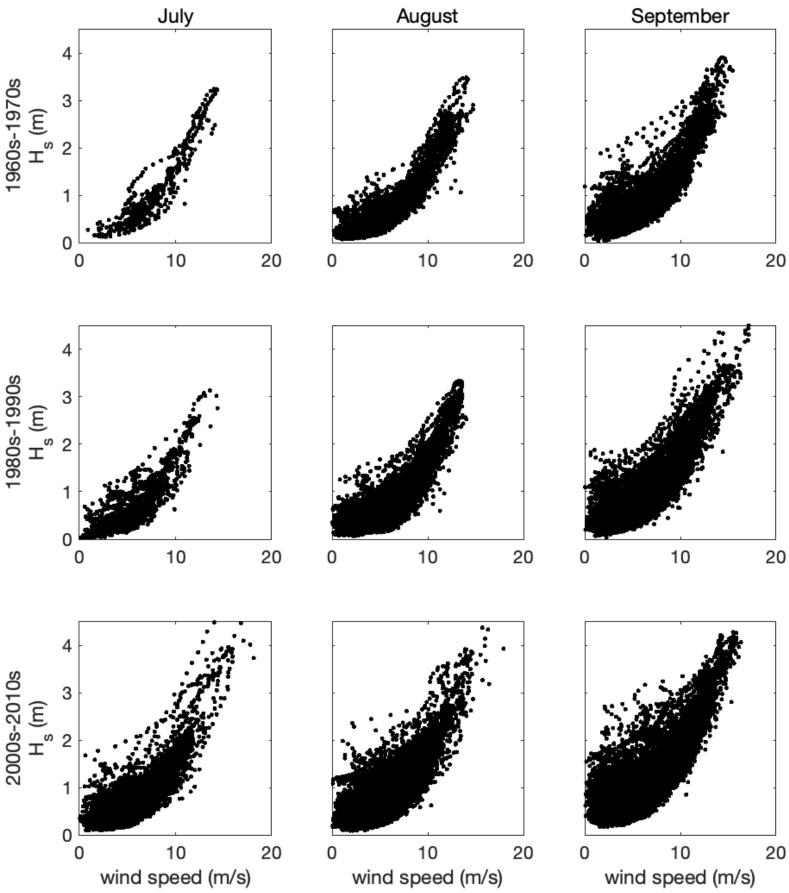

Figure C4: Scatterplots of significant wave heights (for combined wind waves and swell) versus wind speed during summer months. Data are subdivided by 20-year periods.

Appendix D Mooring hardware and sensor configurations

Each mooring deployed in 2022 consisted of a small weighted aluminum frame outfitted with sensors. The two moorings which hosted ADCPs (Nortek Aquadopps; sites T1B and T2B) were then connected by a 25-m ground line to a secondary anchor and an acoustic release/rope-tube assembly which floated about 1 meter above the bed with the aid of a seine float (to avoid fouling). This design minimized flow interference for the ADCP from the release assembly. The other four moorings were simply bottom frames with integrated acoustic release and rope tube, as well as 25-m ground line and secondary anchor to allow for recovery-by-dragging if needed. Moorings were not deployed during the winter due to hazards associated with ice keel scouring. Acoustic releases rather than surface floats were used because floating ice is often present through July and into early August, and can drag moorings and/or cut lines.

Table D1: Sensors and deployment schemes for 2022 moorings (see Table 1). Abbreviations: S = salinity; T = temperature; P = pressure; Tu = turbidity; Vel = velocity (profile); TSS = total suspended solids (derived from turbidity); int = interval.

Station	Parameter(s)	Make	SN	Elevation (cm)	Sampling scheme
T1A	S, T, P	RBR	200154	23	2 Hz, 30 sec, 10 min interval
T1A	Tu	RBR	200154	20	2 Hz, 30 sec, 10 min interval
T1B	Vel, P	Nortek	14938	11	60 sec. avg. int., 30 min samp. int.; waves 1024 samples at 2 Hz (1 MHz sensor)
T1B	TSS	Camp. Sci.	T9110	20[a]	60 sec. avg. int., 30 min samp. int.
T1C	P	RBR	203193	19	16 Hz, 4096 samps, 30 min interval (Wave mode)
T1C	Tu	RBR	203193	22	16 Hz, 4096 samps, 30 min interval
T2A	S, T, P	RBR	200155	23	2 Hz, 30 sec, 10 min interval
T2A	Tu	RBR	200155	20	2 Hz, 30 sec, 10 min interval
T2B	Vel, P	Nortek	14993	20	60 sec. avg. int., 30 min samp. int.; waves 1024 samples at 2 Hz (2 MHz sensor)
T2B	TSS	Camp. Sci.	T9096	20[a]	60 sec. avg. int., 30 min samp. int.
T2C	P	RBR	203194	22	16 Hz, 4096 samps, 30 min interval (Wave mode)
T2C	Tu	RBR	203194	21	16 Hz, 4096 samps, 30 min interval

[a]Mounting elevation was 54 cm above the bed; data were transformed to 20 cm above the bed using a Rouse Profile (see text for discussion).

Appendix E Moored optical backscatter sensor calibrations

Optical backscatter sensors (OBSs) were deployed on all moorings (either packaged within RBR loggers or attached peripherally to Aquadopps). These were calibrated in the laboratory to obtain mass concentration values (in mg/L) from either voltage readings (from the Aquadopp OBSs) or turbidity/NTU readings (from RBR OBSs). To do this, a representative mud mixture collected from the seabed in the bay was mixed in increasingly large concentrations in a bucket, and the concentration of each solution was measured using the field sensors. Water subsamples were collected from the bucket for each concentration and filtered according to the same procedure used for field water samples (see Methods). Linear regressions were then performed with an intercept of zero and applied to the instrument data to obtain measurements of total suspended solids (in g/L) rather than the factory-calibrated nephelometric turbidity units (NTU) or scaled voltages.

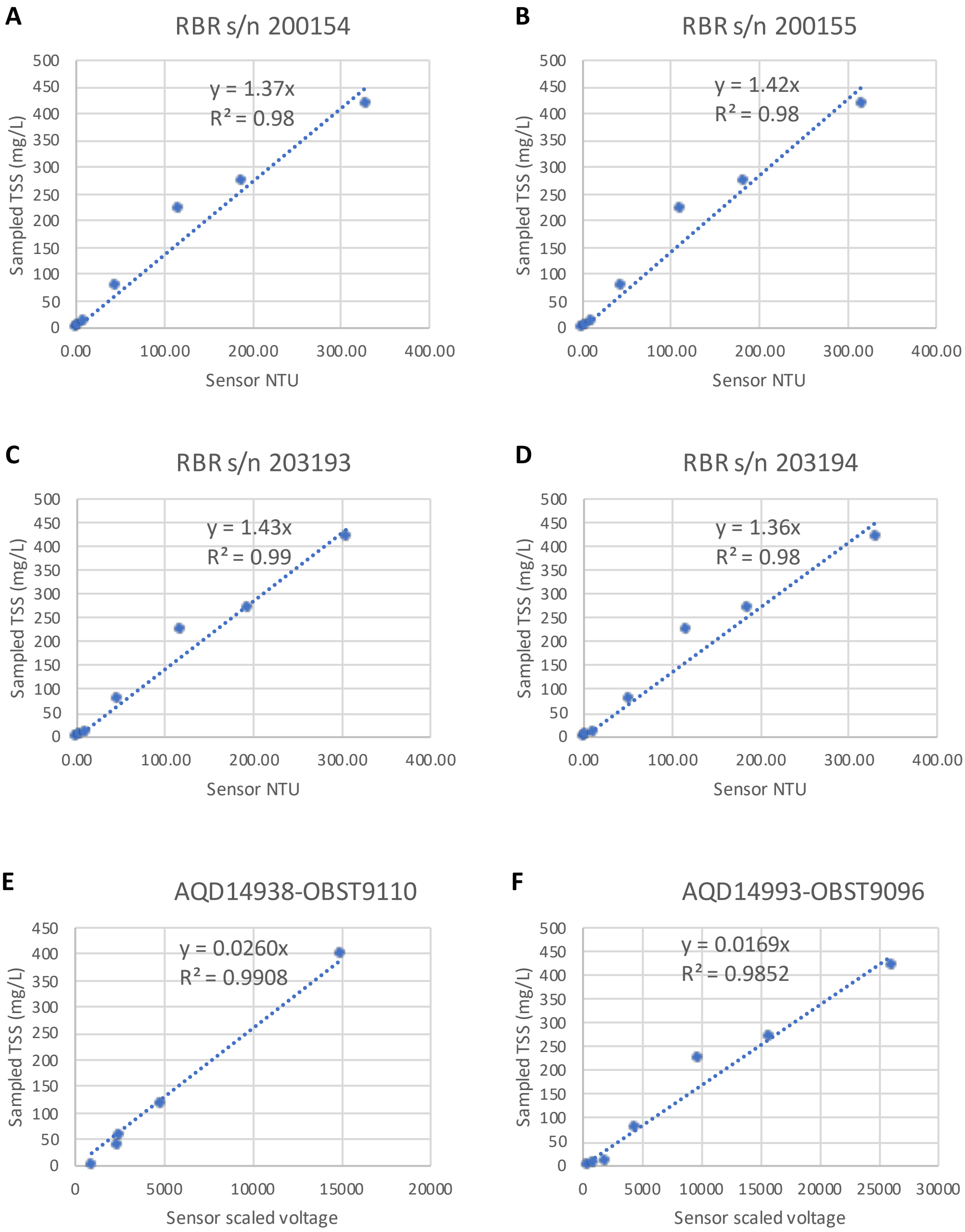

Figure E1: Optical backscatter sensor calibration curves for A) T1A OBS; B) T2A OBS; C) T1C OBS; D) T2C OBS; E) T1B OBS (peripheral to an Aquadopp); and F) T2B OBS (peripheral to an Aquadopp). In A) through D), sensor measurements are reported in NTU in accordance with the RBR supplied internal sensor calibration. In E) and F), sensor measurements are reported as a scaled voltage. Calibrations were performed in July 2023 using sediment from the study area (see text).

Appendix F Rouse Profile

For the T1B and T2A moorings, the OBS data sampled at 54 cmab were converted to measurements at 20 cmab using the Rouse Profile equation. This was done to allow comparisons with OBS data sampled at ∼20 cmab at the "A" and "C" mooring sites. A Rouse profile of suspended-sediment concentration within the bottom boundary layer is simply means an idealized decay profile described by a parabolic diffusivity term (e.g., Boudreau & Hill, 2020):

$$C(z) = C_a(\frac{z}{h-z}\frac{h-z_a}{z_a})^{-w_s/\kappa u_*} \tag{F1}$$

where $C(z)$ is the suspended-sediment concentration (or total suspended solids concentration) at some elevation z, C_a is the measured concentration at some reference height z_a, h is the thickness of the bottom boundary layer (here assumed to be 1 m, though the results are relatively insensitive to this choice), w_s is the sediment settling velocity, κ is von Karman's constant (0.41), and u_* is the total bed shear velocity (see Dey, 2014) which was calculated using a combined wave-current interaction model (see Methods). The sediment settling velocity was calculated using Stoke's Law and a d_{50} value of 11 microns, which was selected based on in situ particle size data.

Appendix G Wave stress calculations

In order to calculate wave-driven bed stresses from ERA5 wave heights and periods, waves were first classified as deep, transitional, or shallow based the peak period and linear wave theory. For deepwater waves, the wavenumber was calculated according to the basic equation $2\times\pi/L$ (where L is the wavelength). For transitional and shallow-water waves, the wavenumber was solved using the standard Newton-Raphson iteration method. The wave-driven bed stress was then calculated according to the following equation:

$$\tau_w = \frac{1}{2}\rho f_w u_{bm}^2 \tag{G1}$$

where τ_w is the bed stress generated by waves, ρ is the water density (assumed here to be 1026 kg/m^3), f_w is a friction factor, and u_{bm} is the maximum wave orbital velocity. The friction factor was calculated following Soulsby (1997):

$$f_w = 1.39 \frac{A}{z_0}^{-0.52} \tag{G2}$$

where A is the semi-orbital excursion (equal to $u_{bm}T/2\pi$, where u_{bm} is the maximum wave-orbital velocity and T is the wave period). The term u_{bm} is calculated as follows:

$$u_{bm} = \frac{\pi H}{T\sinh(kh)} \tag{G3}$$

Helpful discussion of these equations is provided by Soulsby (1987) and Wiberg & Sherwood (2008).

Appendix H Detailed data from T2B mooring and comparison of water levels between T1B and T2B

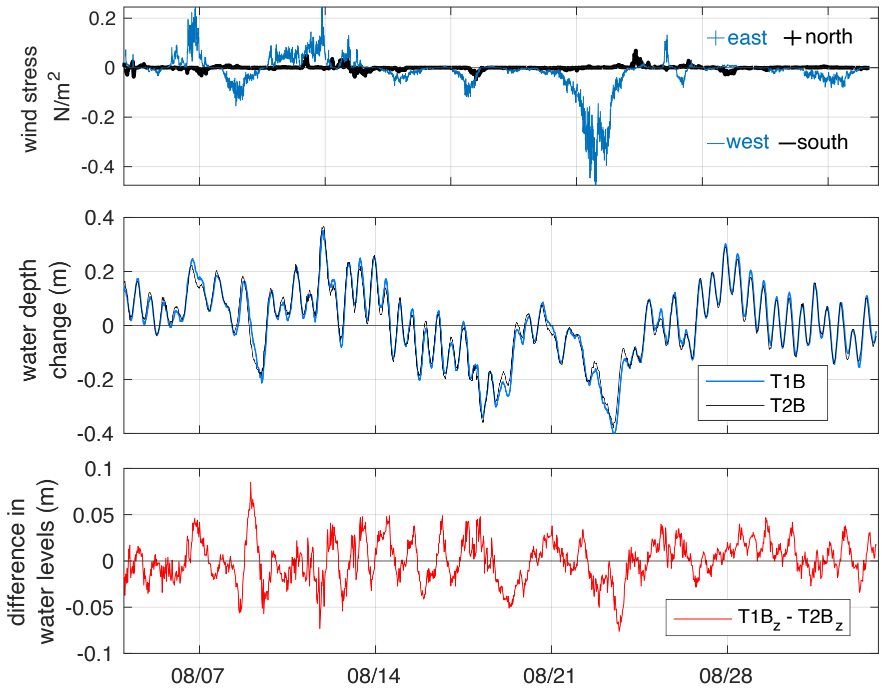

Figure H1: Along-shelf water levels. A) Wind stress (east/west component in blue and north/south component in black). B) Water depth changes at T1B and T2B (relative to the mean depth at each site). C) Difference in water levels (i.e., difference between the two curves in (B)). Positive values mean that water levels were higher at T1B. Negative values mean that water levels were higher at T2B.

931 ## Appendix I Mean currents at T1B

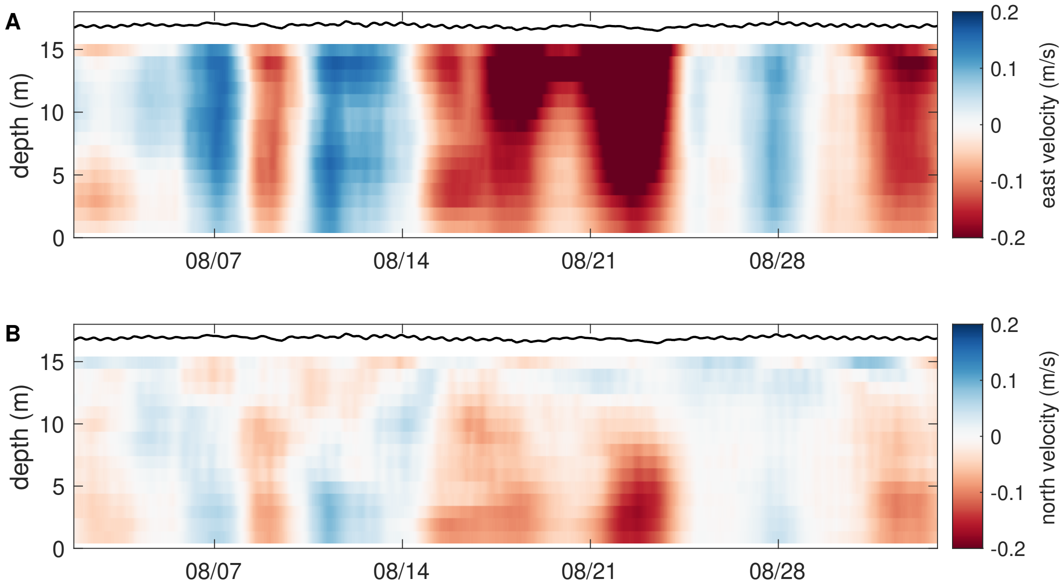

Figure I1: Mean (A) eastward and (B) northward currents at T1B during the 2022 deployment. A moving mean with window equal to four days was applied to velocity data in each depth bin.

Appendix J Wave versus current contributions to bed stress

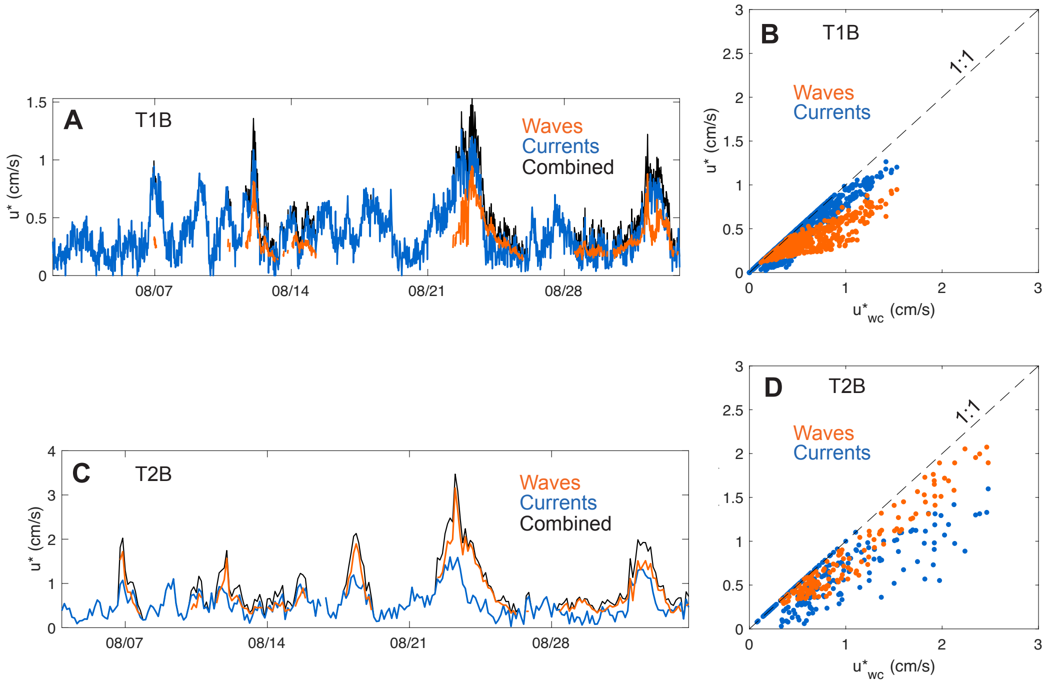

Figure J1: Components of u_* at the "B" mooring sites. A) Time series of wave, current, and combined u_* at T1B. B) Scatterplot of u_{*waves} and $u_{*currents}$ versus total u_* at T1B. C) Same as (A) for T2B. D) Same as (B) for T2B. Note that waves were sampled less frequently at T2B than at T1B (hence the reduced data density).